Supporting Information

Pomeranz-Fritsch Synthesis of Isoquinoline: Gas-Phase Collisional Activation Opens Additional Reaction Pathways

Shibdas Banerjee,[#,†,‖] Fang Liu,[#,†,§,‡] David M. Sanchez,[†,§,‡] Todd J. Martínez,[†,§,‡] and Richard N Zare[*,†]

[†]Department of Chemistry, Stanford University, Stanford, CA 94305, USA. [§]The PULSE Institute, Stanford University, Stanford, CA 94305, USA. [‡]SLAC National Accelerator Laboratory, Menlo Park, CA 94025, USA. [‖]Indian Institute of Science Education and Research Tirupati, Karakambadi Road, Tirupati- 517507, India.

[†]These two authors contributed equally to this work

*Email: zare@stanford.edu

Experimental Details

All necessary chemicals were purchased from Sigma-Aldrich (St. Louis, MO). HPLC grade solvents were purchased from Fisher Scientific (Nepean, ON, Canada).

Synthesis of benzalaminoacetal (non-protonated 1) and 4-(phenylimino)-2-pentanone (non-protonated 8)

The syntheses of these two precursors (non-protonated **1** and **8**) were carried out by a slight modification of the reported protocols.[1,17] 1 mmol benzaldehyde and 1.5 mmol 2,2-dialkoxyethylamine or 1 mmol aniline and 2 mmol acetylacetone were mixed in a 2 mL scintillation vial and heated at 100 ^{0}C for 3.5 h with constant stirring. This procedure formed benzalaminoacetal [Figure S1] or 4-(phenylimino)-2-pentanone [Figure S10], respectively. These precursors were then isolated from the biphasic layer after cooling to room temperature and dried under high vacuum for 24 h. Formation of **1** and **8** was confirmed by electrospray ionization mass spectrometry (ESI-MS) with high mass accuracy (Figures S1 and S10).

Electrospray-assisted synthesis of 4-((2-benzoylphenyl)imino)pentan-2-one and/or ((2-aminophenyl)(phenyl)methylene)pentane-2,4-dione

Unlike the above two reactions, the thermal condensation of 2-aminobenzophenone and acetylacetone was not successful, even after 17 h heating at 100 ^{0}C. However, when we electrosprayed the methanolic mixture of 0.05 mM 2-aminobenzophenone and 0.05 mM acetylacetone, we detected the formation of the condensation product (**13** and/or **20**) by an online mass spectrometer (Figure S11). **13** and/or **20** were indeed found to be formed in electrospray droplets (acidic), which has been extensively studied by us.[2] The existence of the isomeric compounds **13** and **20** in the gas phase is pertinent to the proposed mechanism[3] that these species are the intermediates in the Friedländer synthesis of quinoline by the acid-catalyzed reaction of 2-aminobenzophenone and acetylacetone.

ESI-MS Experimental Conditions

0.05 mM methanolic solution of the analyte was electrosprayed using a home-built ESI source (Figure S2) in positive ion mode (+5 kV) at a flow rate of 1 µL/min through silica tubing (100 µm i.d.) with a coaxial sheath gas flow (N_2 at 120 psi). The mass spectrometer inlet capillary temperature was maintained at approximately 275 °C, and capillary voltage was kept at 44 V. The spray distance (the on-axis distance from spray tip to the entrance of the heated capillary) was

maintained at 1.5 cm. All experiments were carried out under identical conditions, unless otherwise stated, to detect the product by a high-resolution mass spectrometer (Thermo Scientific LTQ Orbitrap XL Hybrid Ion Trap-Orbitrap mass spectrometer). Helium was used as the collision gas in the collision-induced dissociation cell (CID cell; an ion trap as shown in Figure S2). CID spectra (MS^2 and MS^3) were acquired using an isolation width of 0.9 *m/z* units. The activation Q (as labeled by Thermo Scientific, used to adjust the q_z value[4] for the precursor ion) was set at 0.25, and the activation time employed was 30 ms at each CID stage. The normalized collision energy (NCE)[5] was set between 15 % and 25 % for multi-stage CID experiments (MS^n) and it was varied from 0 % to 60 % for the dissociation profile (breakdown) study of the mass-selected ion. Data acquisition was performed for 1 min using XCalibur software (Thermo Fisher Scientific).

Computational Details

Theoretical calculations for the synthesis of isoquinolines were carried out using the TERACHEM[8] and Q-Chem[9] software suites. All calculations were initially performed at the B3LYP level with the 6-31G basis set. The effect of the chosen basis set was investigated by computing the reaction barrier for reaction step **1→5** in the Pomeranz-Fritsch synthesis with 6-31G*, 6-31G**, 6-31+G*, and cc-PVDZ basis sets, which resulted in changes of at most 2 kcal/mol. In addition, B3LYP results were compared to PBE0, ωPBEh ($\omega = 0.2$), ωB97X, and B3P86. This wide range of functionals leads to differences which are not expected to have much effect on the identification of the rate determining step (e.g., a barrier height of 44 kcal/mol was changed by 1-6 kcal/mol). A graphical summary is provided in Figure S22. For each step of the fragmentation reactions, the reaction pathway calculation was not restricted to the traditional calculation from a single minimized reactant structure to a single minimized product structure. Instead, all possible reaction pathways starting from different conformers of the reactant to conformers of the product were explored with our newly developed Python program AUTONEB. The pathway exploration process worked as follows: for each reactant or product molecule, starting from an initial conformer, AUTONEB generated new geometries by rotating dihedrals in the molecule. All geometries were then automatically sent to TeraChem for minimization. The minimized geometries were then pruned in four steps. First, optimized geometries whose SMILES (simplified molecular input line entry system) codes differed from the original molecule were detected and rejected. Second, all geometries more than 100 kcal/mol above the most stable structure were excluded. Third, surviving conformers were clustered based on the RMSD of the conformer's distance matrix

spectrum. Fourth, the lowest energy geometry in each cluster was selected to represent a stable conformer for a particular intermediate. The reaction pathways linking each pair of reactant conformer and product conformer were then calculated with the zero-temperature string method.[10,11] The nudged elastic band (NEB) method[12] with climbing image was used to refine the featured paths, path-L and path-S, of each reaction step. The climbing image NEB (CI-NEB) provides a more accurate transition state (while the zero-temperature string method is concerned with the reaction path and not with providing an accurate estimate of the transition state). A larger 6-31G** basis set was used in this CI-NEB refinement. The climbing image structures were confirmed to be genuine minima or transition states by frequency analysis with Q-Chem for each reaction step in Pomeranz-Fritsch reaction network. In particular, a transition state was deemed valid when the computed imaginary frequency was greater than 100 wavenumbers from its nearest mode. Thermochemistry corrections were applied to each product, transition state, and reactant structures to account for enthalpic and entropic contributions to reaction barriers. Energies (ΔG values) are reported as the sum of electronic energy and thermochemical contributions (298K) calculated in the harmonic approximation from normal mode analysis.

Supplementary Note S1

In CID, a gaseous molecular ion collides with a neutral and unreactive gaseous target (*e.g.*, helium, nitrogen, or argon).[13,14] As a result, energy is gained and redistributed among different vibrational degrees of freedom (internal energy) within the ion, causing unimolecular fragmentation to occur.[14] The collisional activation may involve rapid energy deposition under single-collision conditions and at short interaction times, or it might be a relatively slow process, as in multiple collisions. If the activation step takes place within a vibrational period (single collision), the ion cannot have scope for undergoing the rearrangement reaction in the gas phase.[14] However, if activation proceeds in stepwise fashion, as in multiple collisions and the time between the activation steps is long relative to vibration, interesting bond rearrangements and degradation chemistry can happen, which is substantiated by a number of literature reports.[15-20]

Supplementary Note S2

Combes quinoline synthesis in the gas phase

The Combes quinoline synthesis[21-23] is another type of acid-catalyzed synthesis of quinoline (Scheme S2) by the condensation of aniline and a β-diketone (such as acetyl acetone). In the solution phase, the synthesis is carried out in two steps.[23] The first step involves the formation of a Schiff base (4-(phenylimino)-2-pentanone) by the reaction of aniline and acetylacetone. In the second step, acid (*e.g.*, sulfuric acid) is added and the Schiff base tautomerizes to form an enamine, which undergoes in situ annulation followed by water elimination to form the 2,4-substituted quinoline *via* different intermediates as shown in Scheme S2. In the present study, we separately prepared the Schiff base 4-(phenylimino)-2-pentanone (see Experimental section) and electrosprayed it from a methanolic solution to produce the protonated Schiff base **8** in the gas phase (Figure S10). On collisional activation, **8** transformed into protonated 2,4-dimethylquinoline **12** as evidenced by the product ion signal at *m/z* 158.0954 (Figure S12), which was also verified by comparing with the CID-MS^2 spectrum of the standard protonated 2,4-dimethylquinoline (Figure S13). No other product ion was observed in the MS^2 spectrum of **8** (Figure S12). Therefore, this gas-phase quinoline synthesis pathway from the precursor **8** can be described in terms of the analogous pathway proposed to be associated with the solution-phase Combes quinoline synthesis (Scheme S2). The upper panel of Figure S12 shows the transformation of **8** into **12** *via* different isomeric intermediates (**9**-**11**), which are analogous to the intermediates observed in solutions (Scheme S2). Being isomeric in nature, the precursor **8** and intermediates **9**-**11** could not be distinguished by their *m/z* value (176.1060). However, theoretical calculation supported the formation of these intermediates (**9**-**11**) in an energetically favorable pathway (*vide infra*). Although, the formation of **12** from **8** can be successfully interpreted by the reaction route associated with solution-phase counterpart (Scheme S2), it does not rule out the possibility of other unknown mechanisms. Nevertheless, unlike the Pomeranz–Fritsch reaction (Figure 1), the lack of the evidence of any intermediates with distinct *m/z* values does not unambiguously suggest any other parallel route of the reaction in the gas phase.

The energy-resolved mass spectrometric study, shown in the breakdown curve of **8** (Figure S14), suggested that abundance of **12** increases with increasing NCE and reaches a plateau at NCE ~55 %. Therefore, unlike the gas-phase Pomeranz-Fritsch synthesis of isoquinoline (Figure 2a),

moderately high collision energy was required to yield the maximum amount of product **12** by gas-phase Combes quinoline synthesis. This result is consistent with theoretical calculations, which showed a higher activation energy barrier of the rate-determining step in Combes quinoline synthesis than that in the Pomeranz-Fritsch synthesis of isoquinoline in the gas phase (*vide infra*).

CID was also performed on the deuterated **8** (**8D**) and formation of both protonated product **12** and deuterated product **12D** was detected in the MS^2 spectrum of **8D** (Figure S15). This result indicates again the involvement of the 'mobile proton model'[24,25] that causes H/D exchange in the activated states of precursor **8D** and intermediates **9D**-**11D** to yield both **12** and **12D**.

As shown in Table S3, the theoretical results for the Combes quinoline synthesis are much simpler compared to the Pomeranz-Fritsch reaction. There is only one route from the initial reactant **8** to final product **12**. Figure S16 shows its energy profile. The rate determining step is the ring closure, **9→10**, with an activation energy 22.9 kcal/mol, which is significantly higher than the 13.54 kcal/mol of Pomeranz–Fritsch synthesis. This is consistent with our experimental result that moderately high collision energy was required to yield the maximum amount of product **12**.

Supplementary Note S3

Friedländer synthesis of quinoline in the gas phase

The Friedländer synthesis[3,26] is also an acid-catalyzed process for production of quinoline from *o*-aminoaryl aldehydes or ketones (such as 2-aminobenzophenone) and a ketone (such as acetylacetone). The reaction is believed to proceed through two parallel routes (see Scheme S3).[3] In the first route, 2-aminobenzophenone and acetylacetone react in a rate-limiting step to form an *α*,*β*-unsaturated carbonyl compound *via* an aldol adduct followed by water elimination (Scheme S3). This *α*,*β*-unsaturated carbonyl compound then undergoes ring closure, by means of a Schiff base formation reaction to yield a substituted quinoline by the elimination of another water molecule. In the second route, a Schiff base is formed from the condensation reaction of 2-aminobenzophenone and acetylacetone by the elimination of water followed by the intramolecular aldol condensation to yield the same substituted quinoline by eliminating another water molecule (Scheme S3).

Although the thermal condensation of 2-aminobenzophenone and acetylacetone was not successful, even for 17 h heating at 100 ^{0}C, we electrosprayed the mixture of above the two compounds from a methanolic solution[2] and detected the ion signal at *m/z* 280.1340 (Figure S11), which corresponds to the two isomeric species, protonated Schiff base **13** and/or the protonated *α*,*β*-unsaturated carbonyl compound **20**. The details of this electrospray-assisted synthesis of **13** and/or **20** have been discussed in the Experimental Section.

CID on the precursor species **13**/**20** exhibited (Figure S17) the formation two product ions corresponding to the gas-phase syntheses of two substituted quinolines **16** (in protonated form, *m/z* 220.1110) and **19**/**22** (in protonated forms, *m/z* 262.1214). Indeed, the formation of the product **19**/**22** (Figure S17) was confirmed by CID of the standard protonated 2-methyl-3-acetyl-4-phenylquinoline (Figure S18). Although the formation of **19**/**22** can be attributed to reaction routes (top panel of Figure S17) analogous to that in solution (Scheme S3), generation of **16** cannot be interpreted that way (Scheme S3). Therefore, formation of **16** indicates that intermediate **14** has undergone loss of neutral acetic acid to yield **16** in the gas phase. Thus, the reaction route **13→14→15→16** is unique on collisional activation of **13**. Although the precursors (**13** and **20**) and intermediates (**14**, **15**, **17**, **18**, **20**, and **21**) are isomeric in nature and cannot be distinguished by their identical *m/z* value (280.1320), theoretical calculations supported their formation (vide

infra), and the production of **16** unambiguously suggests the involvement of **15** as an intermediate in the reaction (**13→14→15→16**; Figure S17).

The energy-resolved mass spectrometric study, shown in the breakdown curve of **13**/**20** (Figure S19), suggested that abundance of protonated quinolines **16** and **19**/**22** increases with an increase in NCE and reaches a plateau at NCE ~16 %. The abundance of the product **16** was always found to be higher than that of **19**/**22** upon collisional activation of **13**/**20** at different collision energies (Figure S19).

CID was also performed on the deuterated **13**/**20** (**13D**/**20D**) and formation of both protonated products (**16** and **19**/**22**) and deuterated products (**16D** and **19D**/**22D**) was detected in the MS^2 spectrum of **13D**/**20D** (Figure S20). This result again indicates the involvement of the 'mobile proton model'[24,25] that induces H/D exchange in the activated states of the precursors **13D** and **20D**, and intermediates **14D**, **15D**, **17D**, **18D**, and **21D** to yield the products (**16**, **16D**, **19**, **19D**, **22**, and **22D**; Figure S20).

Figure S21 shows the energy profile of the three different routes of the Friedlander synthesis of quinoline in the gas phase (Table S4) as depicted in Figure S17. Routes (a) and (b) both start from the protonated Schiff base **13**, but result in different products **16** (*m/z* 262.1214) and **19** (*m/z* 220.1110), respectively. Route (c) starts from the protonated *α*,*β*-unsaturated carbonyl compound **20,** and results in the product, **22**, indistinguishable from **19** by *m/z*. CID experiment shows that the abundance of the product **16** was always found to be higher than that of **19**/**22**. An explanation for this behavior might be as follows. Routes (a) and (b) branch after reaching **14**. Focusing on path-L, it seems that (b) is energetically slightly more favorable than (a), because the r.d.s. barriers for **14→15→16** and **14→17→18→19** are 31.9 kcal/mol and 28.5 kcal/mol. However, such analysis (with only path-L) is obtained with the assumption that, for each step of the reaction, the barrier between the reactant conformers for path-S and path-L is much lower than the barrier from reactant to product. In fact, the barrier for the transformation between conformers could be so high that only path-S dominates the reaction. If that is the case, then (b) may be less preferred because the step **17→18** has a much higher barrier of 81.1 kcal/mol for path-S than any step in (a). Therefore, for the fragmentation of **13**, it is possible that more **16** is obtained than **19.** Route (c) overall has a significantly lower reaction barrier of less than 10 kcal/mol. However, its initial reactant, **20** (absolute energy -901.206298 Hartree)**,** is much less stable than **13** (-

901.230088 Hartree) by 14.9 kcal/mol. Therefore, at the experimental temperature (298 K), the initial reactant seems more likely to be **13** instead of **20**. Thus, the majority of the reactions going on would be through routes (a) and (b) instead of (c). All these facts could render the higher abundance of **16** than **19/22** a reasonable phenomenon.

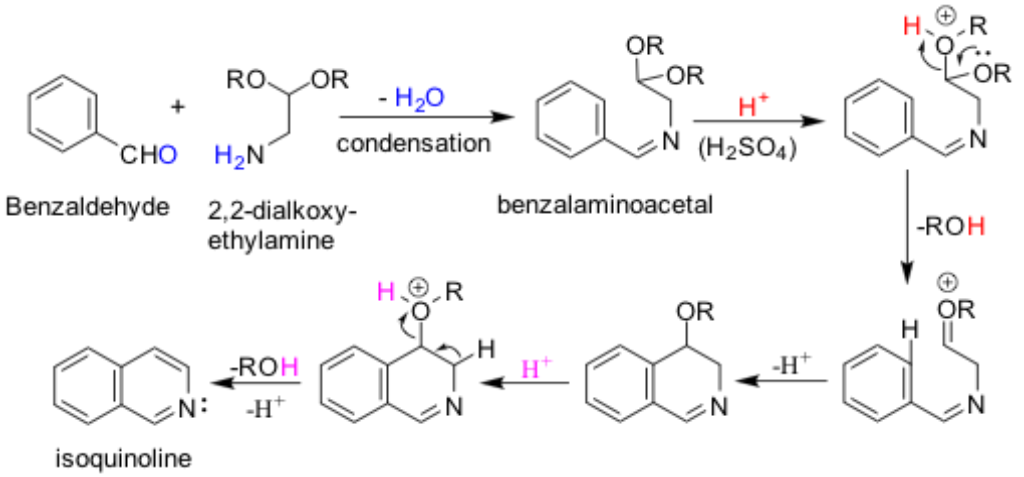

Scheme S1. Pomeranz–Fritsch synthesis of isoquinoline in solution

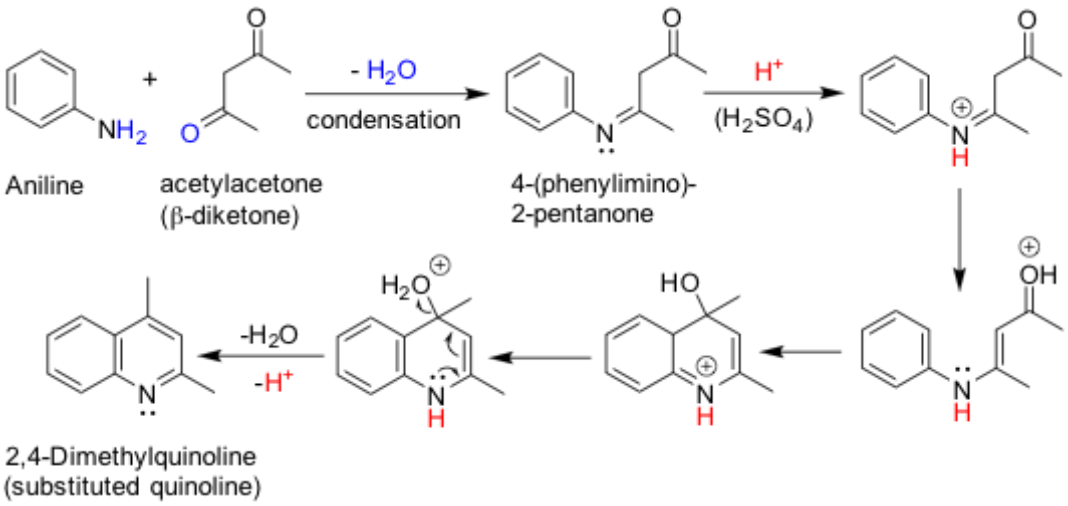

Scheme S2. Combes quinoline synthesis in solution

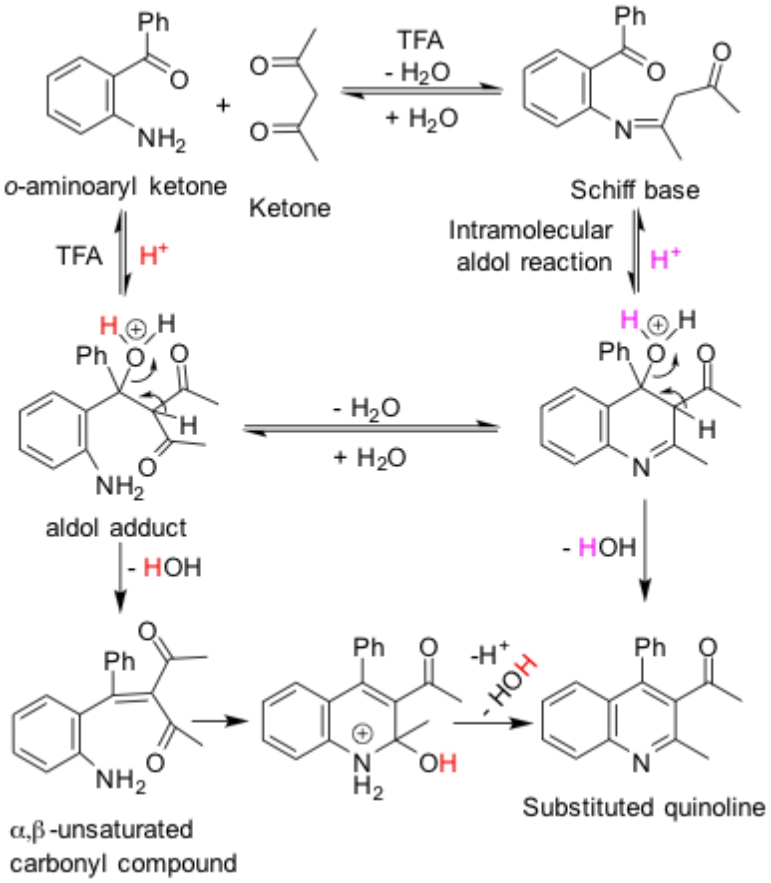

Scheme S3. Friedländer synthesis of quinoline in solution

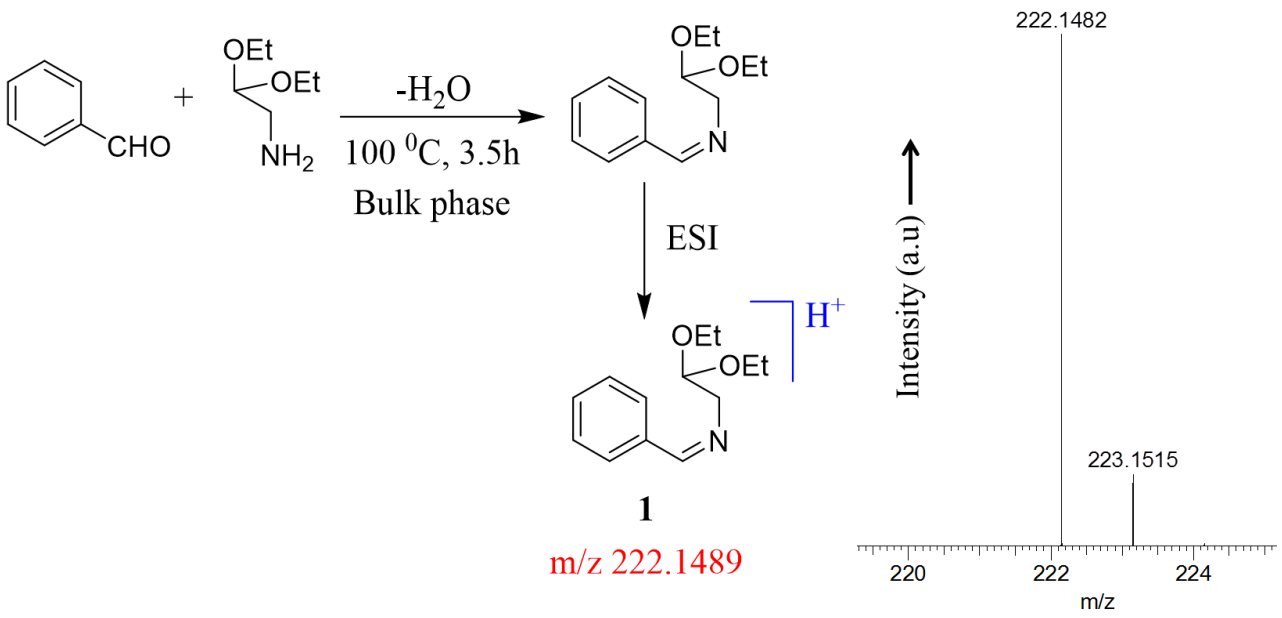

Figure S1. Synthesis of the benzalaminoacetal in bulk phase followed by electrospray ionization (ESI) to generate the gaseous protonated species **1**, which was detected (right panel ESI-MS) by a high-resolution mass spectrometer. The theoretical *m/z* 222.1489 (in red) for **1** agrees well with the experimentally observed *m/z* 222.1482 for the same species (right panel).

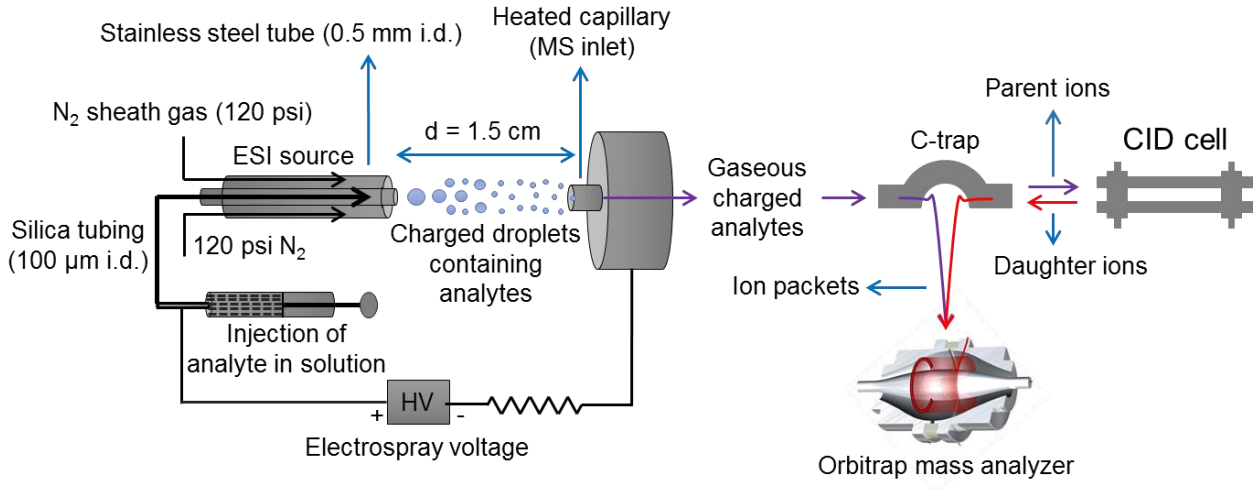

Figure S2. Schematic diagram of the electrospray ionization process followed by collision-induced dissociation (CID) of the gaseous precursor ion to fragment into product ions for their subsequent analysis by an orbitrap mass analyzer.

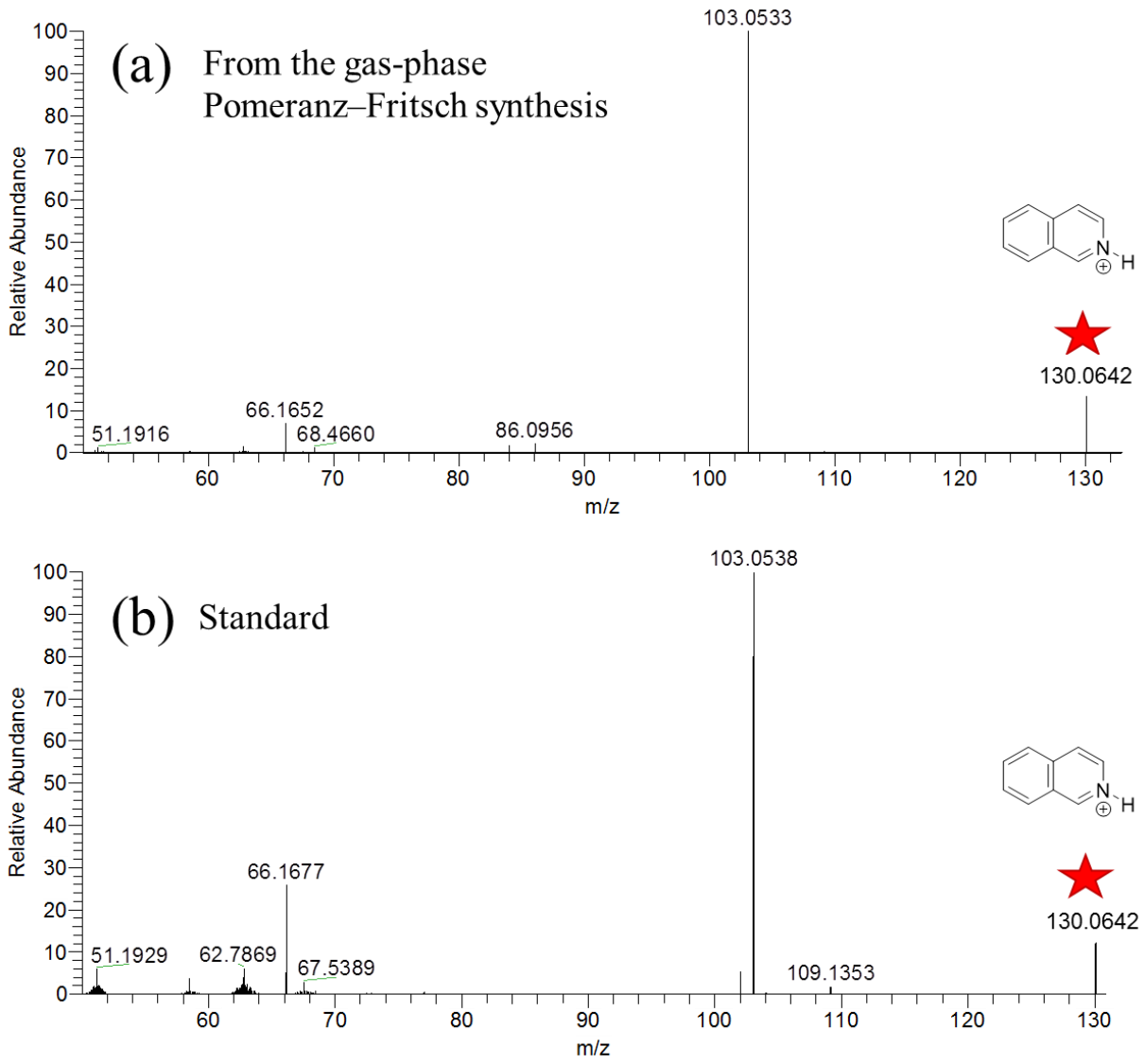

Figure S3. Collision-induced dissociation on the species at *m/z* 130.0642 obtained from (a) the gas-phase Pomeranz-Fritsch synthesis of isoquinoline (Figure 1), and (b) standard isoquinoline. A star marks the activation of the precursor species by CID.

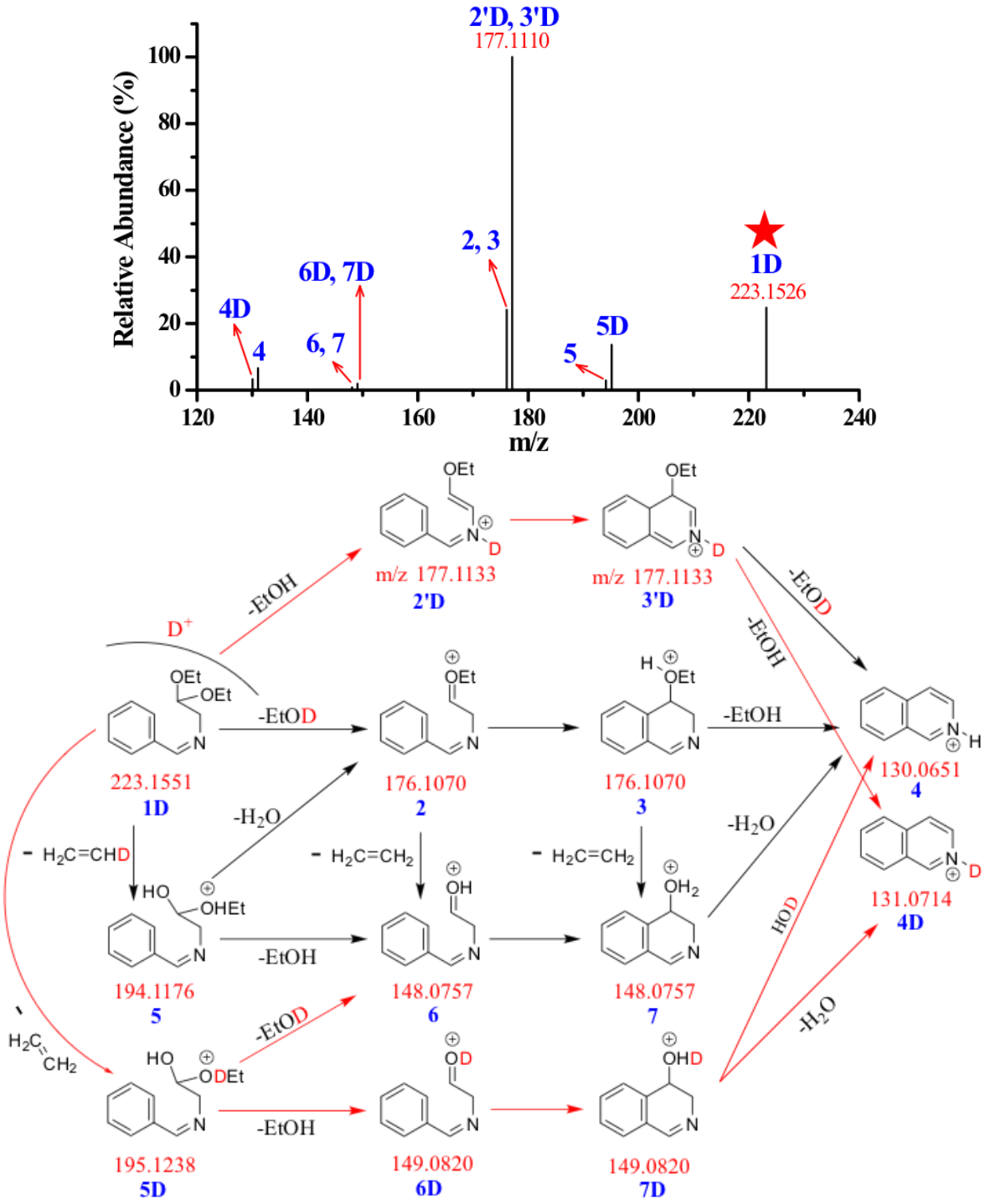

Figure S4. CID-MS2 of deuterated **1** (**1D)** (*m/z* 223.1526), which produced different deuterated species (**2′D**, **3′D**, and **4D**-**7D**; D represents that the species is deuterated) as well as protonated species (**2**-**7**) following 'mobile proton model' as presented in the lower panel Scheme. A star marks the activation of the precursor species by CID. The theoretical *m/z* values of all species are given in red below their structures in the scheme. The reaction routes in red arrows were not detected from CID of protonated **1** (see Figure 1) but from deuterated **1** (**1D**).

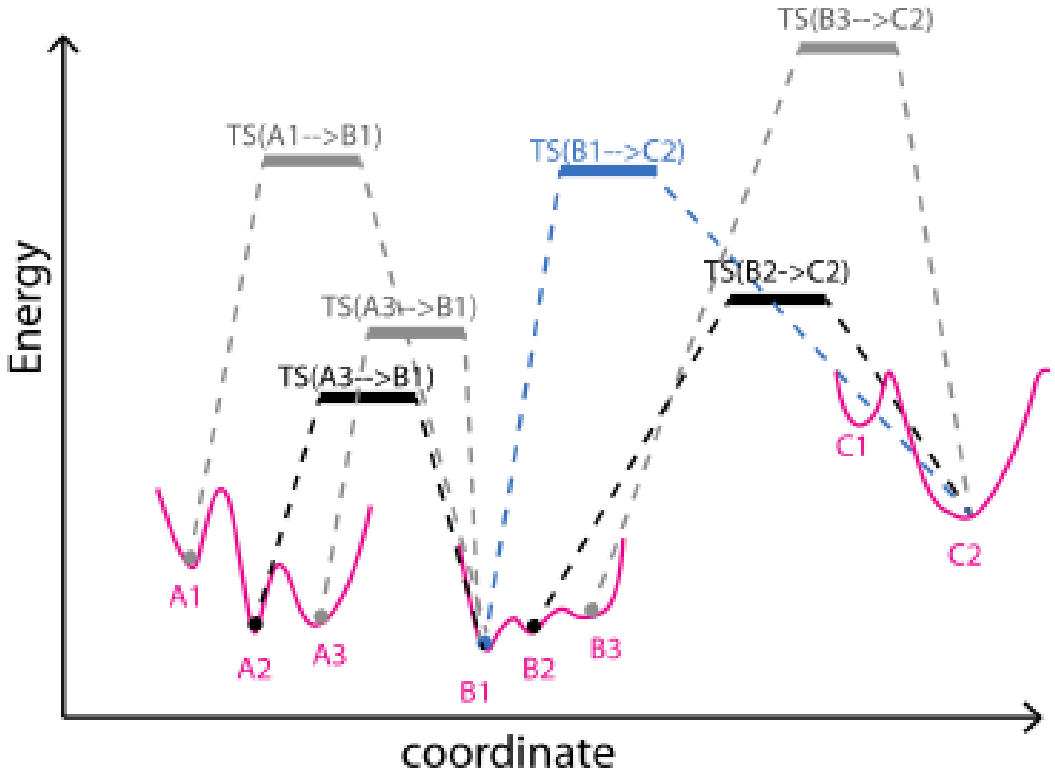

Figure S5. Schematic of the backtracking analysis used in the reaction pathway calculation involving multiple conformers. Pink curves represent the conformational landscape of reaction species. Horizontal bars indicate the energy of the transition state structures. The bars and dashed lines indicate the paths linking the reactant and product conformers. The lowest barrier path (path-L) is black while the most stable reactant path (path-S) is blue. Other paths are grey.

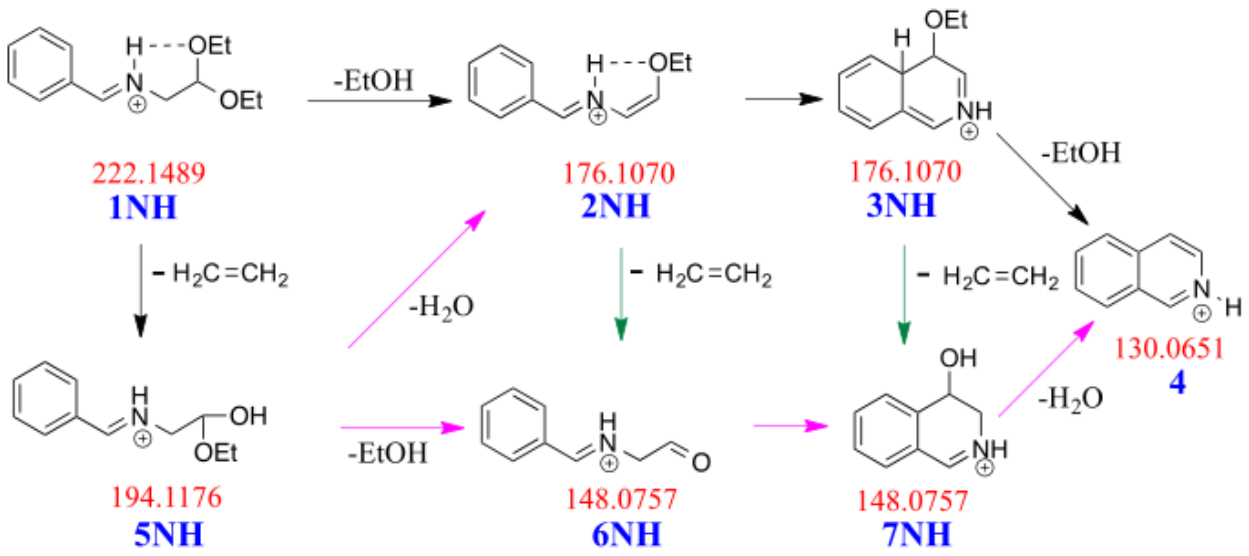

Figure S6. The gas-phase Pomeranz–Fritsch synthesis from the nitrogen-protonated precursor. The theoretical *m/z* values of all species are given in red below their structures in the scheme.

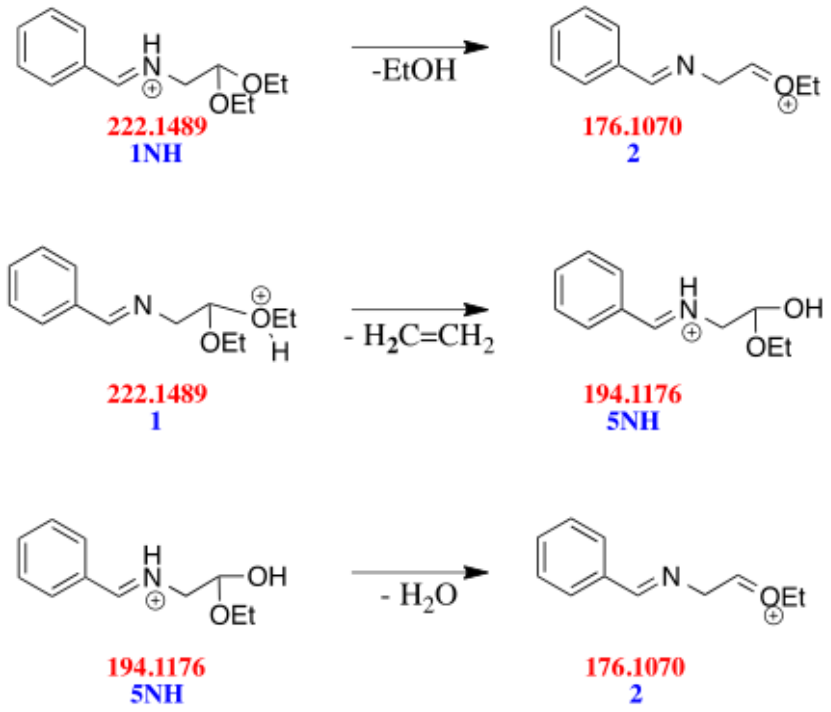

Figure S7. Proton transfer pathways in the gas-phase Pomeranz–Fritsch synthesis network. The theoretical *m/z* values of all species are given in red color their structures in the scheme.

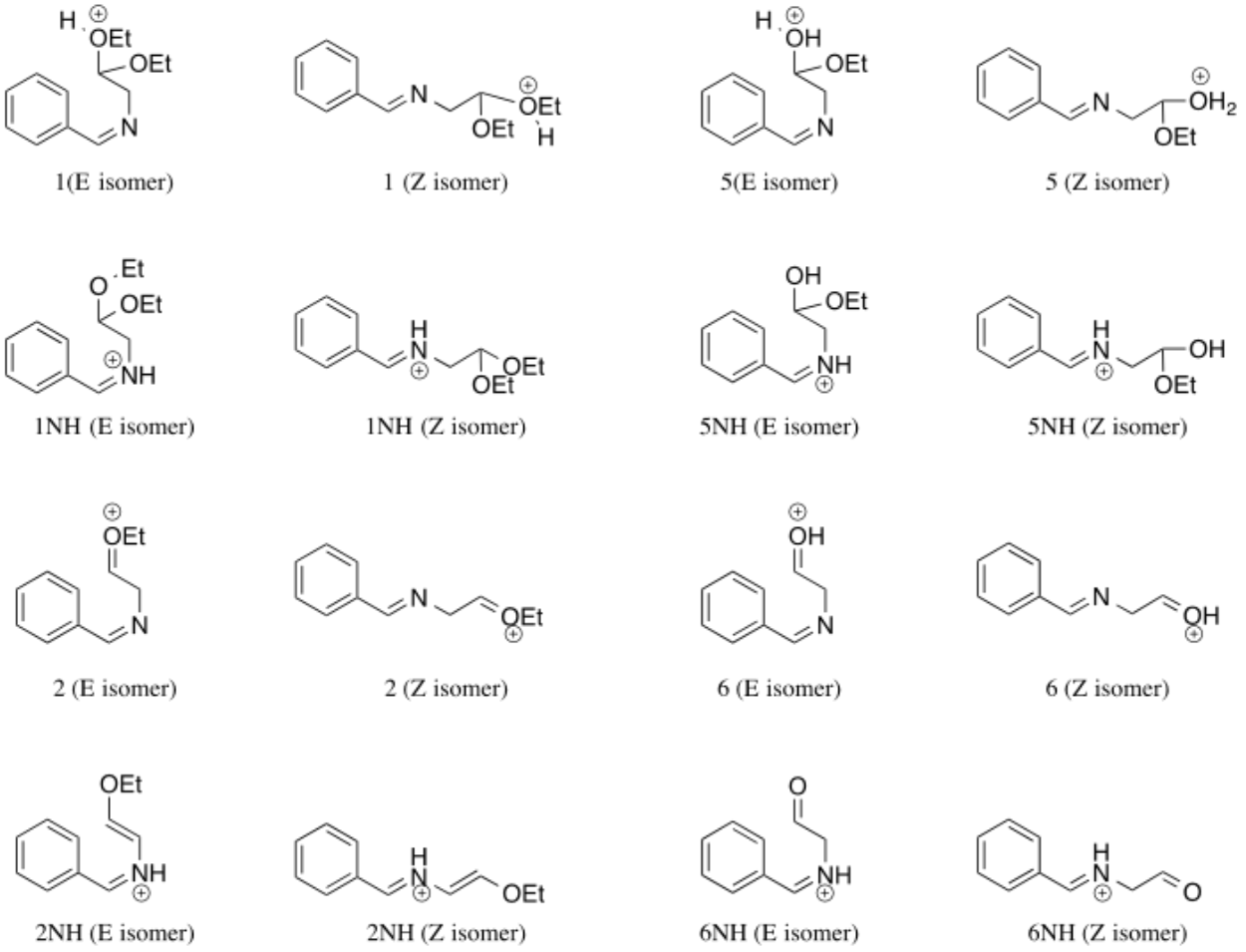

Figure S8. Z and E conformers of species in the gas-phase reaction network of the Pomeranz–Fritsch synthesis of isoquinoline.

Figure S9. Energy profiles (ΔG given in red in kcal/mol) for the gas-phase Pomeranz–Fritsch synthesis in the route:

(a) **1→2→3′→3→7→4**

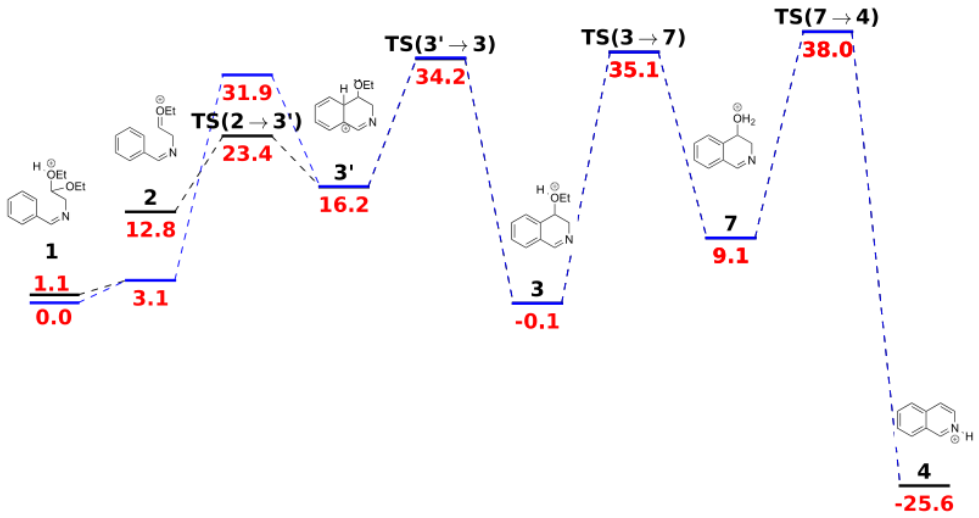

(b) **1→5→2→3′→3→4**

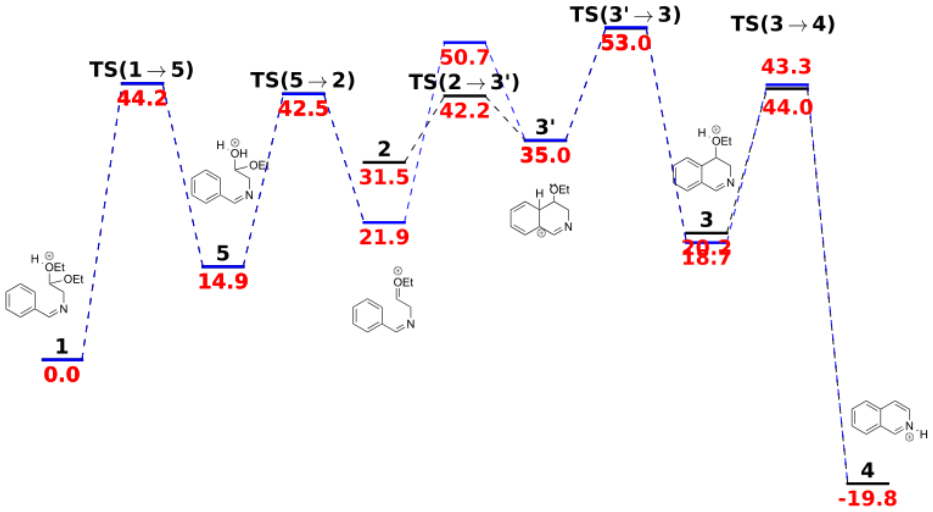

(c) **1→5→2→3′→3→7→4**

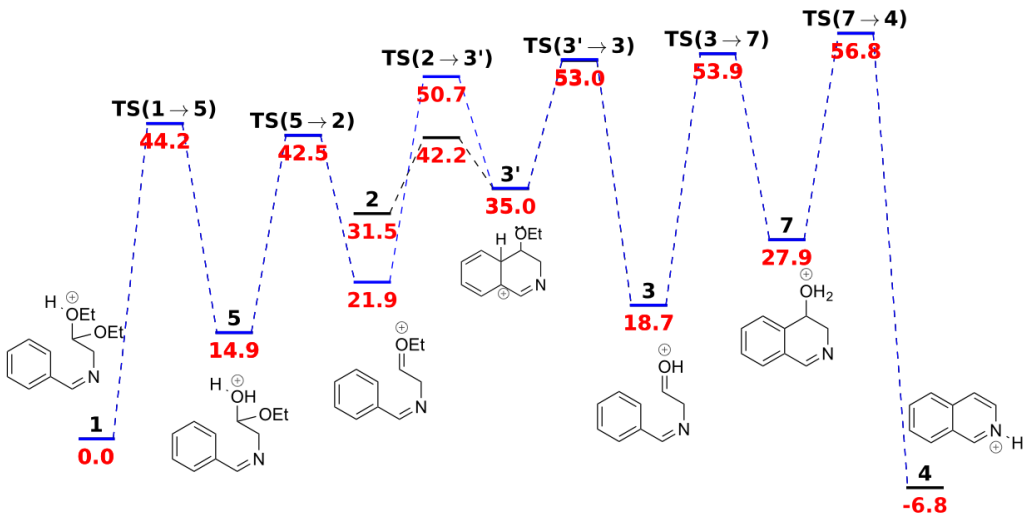

(d) **1→5→2→6→7→4**

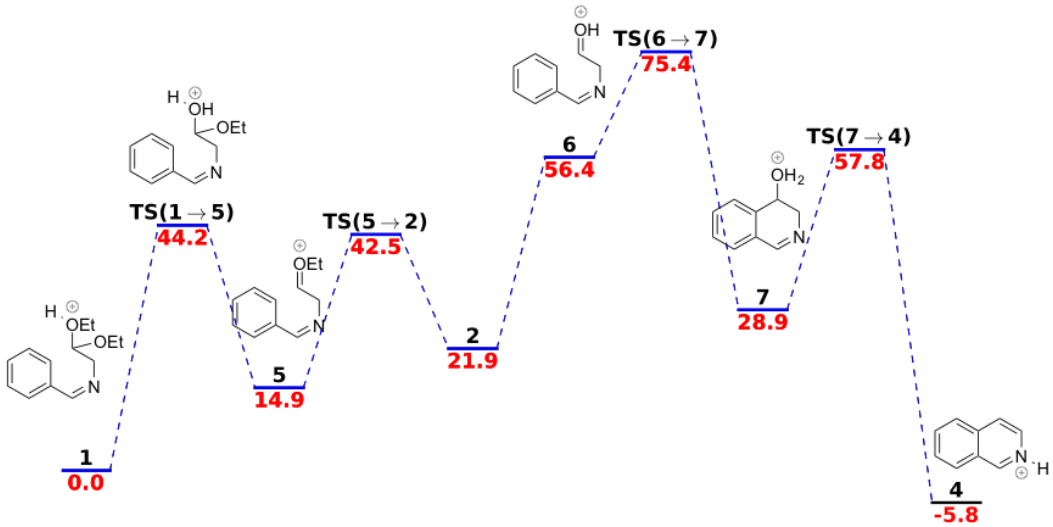

(e) **1→5→6→7→4**

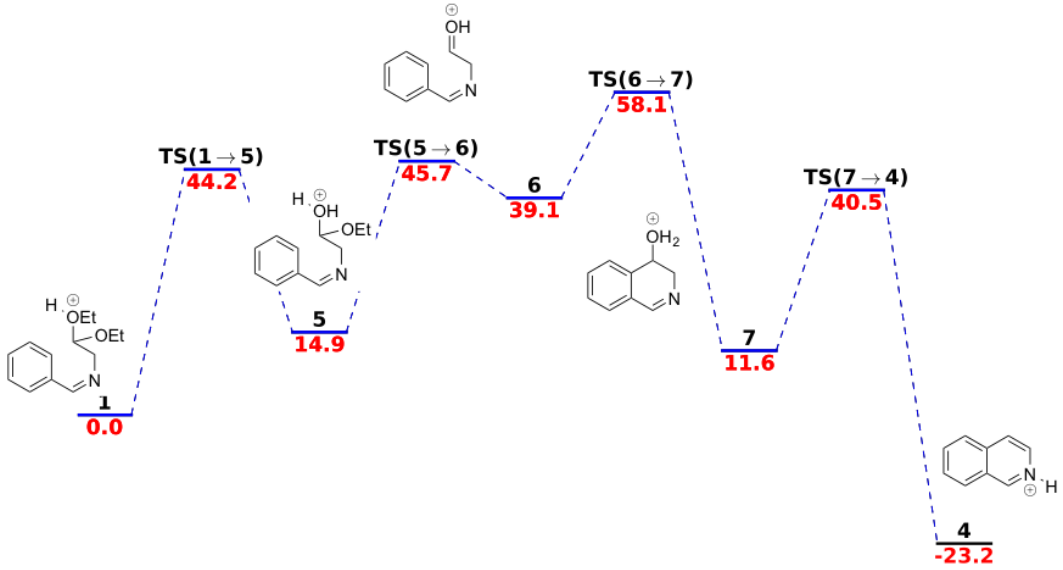

(f) **1→5NH→2→3'→3→7→4**

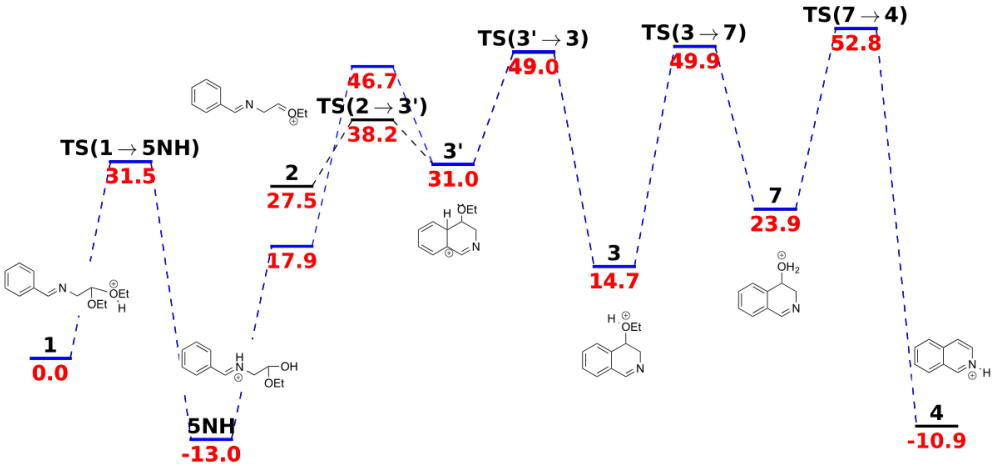

(g) **1→5NH→2→6→7→4**

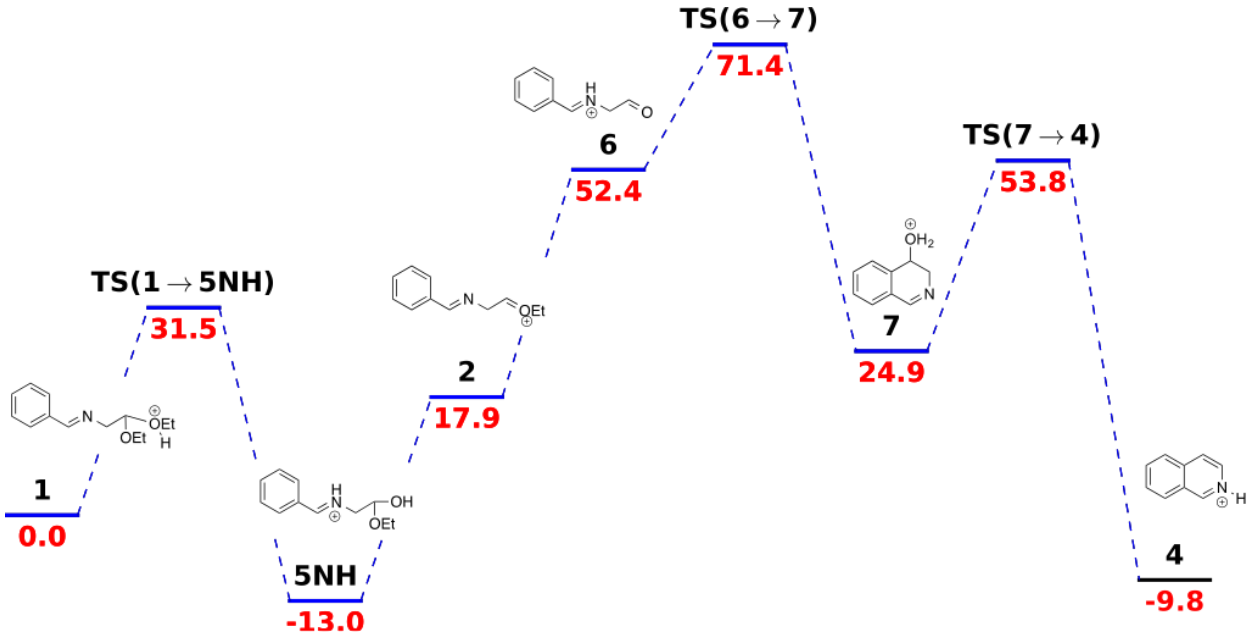

(h) **1→5NH→2NH→3NH→4**

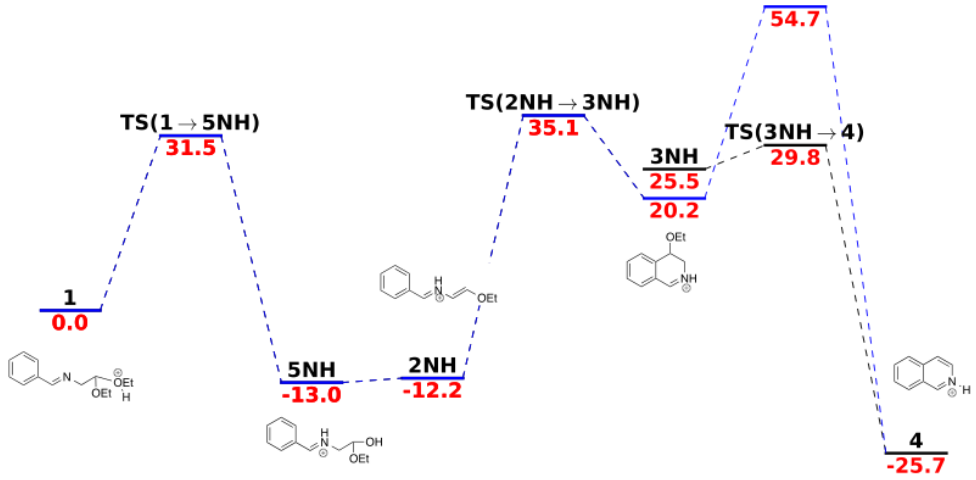

(i) **1→5NH→2NH→6NH→7NH→4**

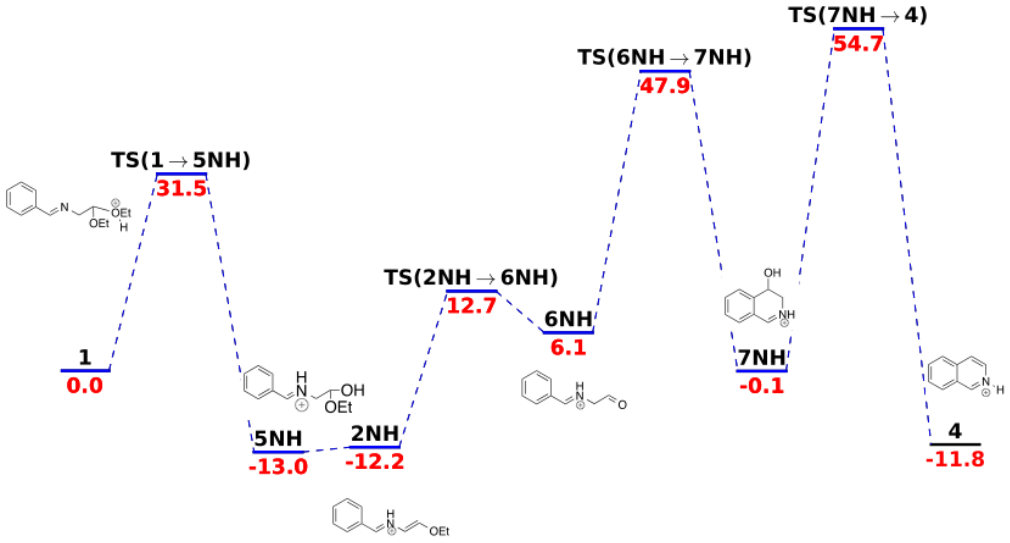

(j) **1→5NH→2NH→3NH→7NH→4**

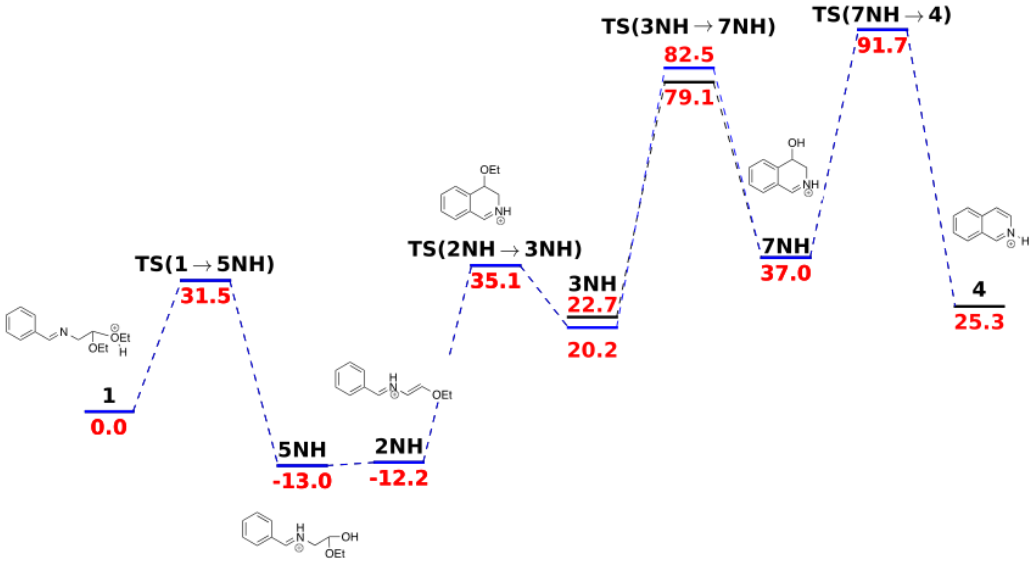

(k) **1→5NH→6NH→7NH→4**

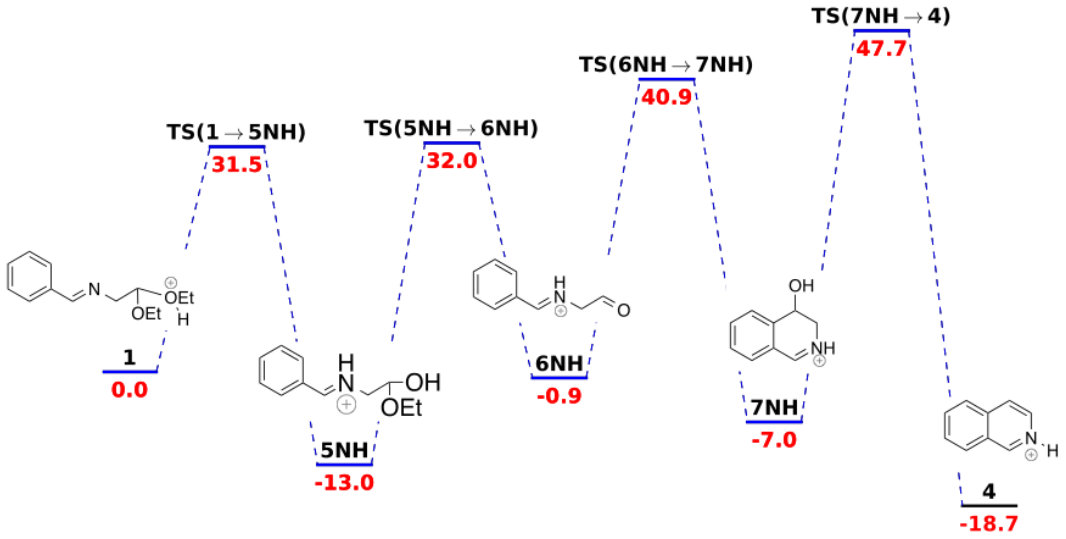

(l) **1NH→2→3'→3→4**

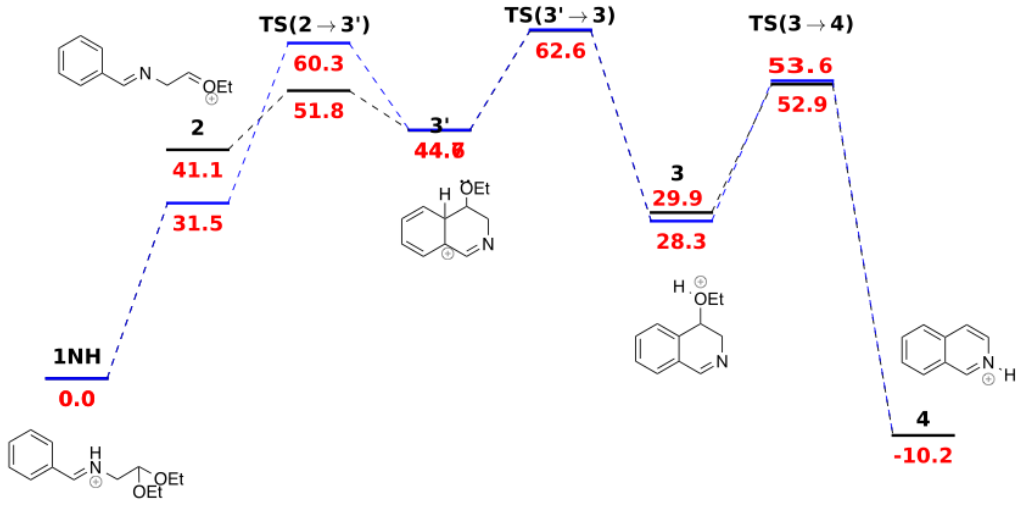

(m)**1NH→2→3'→3→7→4**

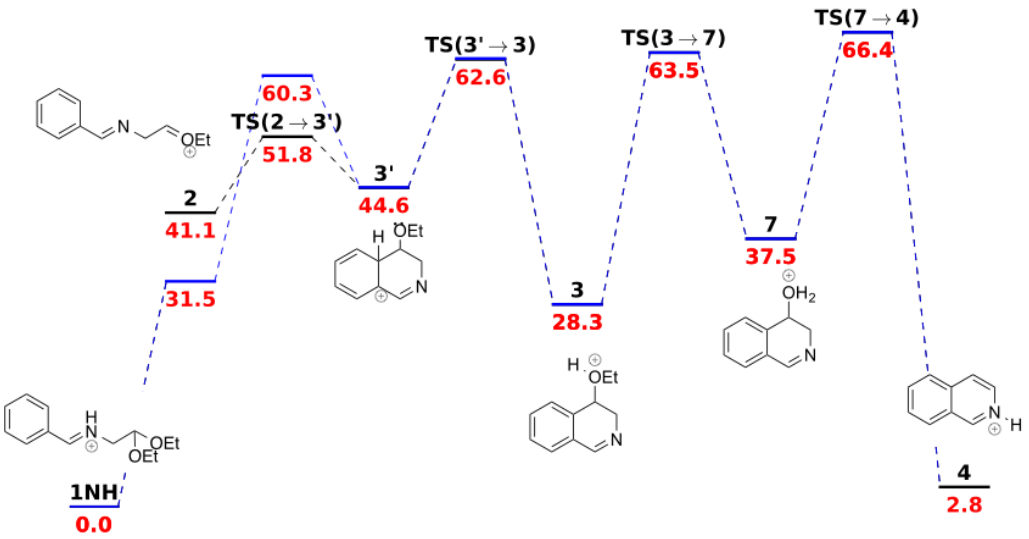

(n) **1NH→2→6→7→4**

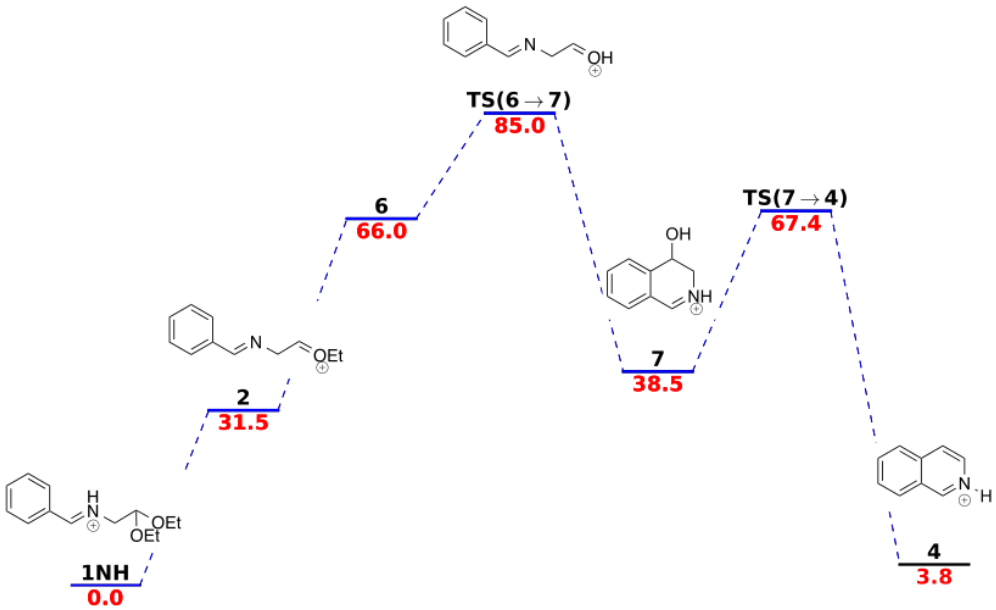

(o) **1NH→2NH→3NH→4**

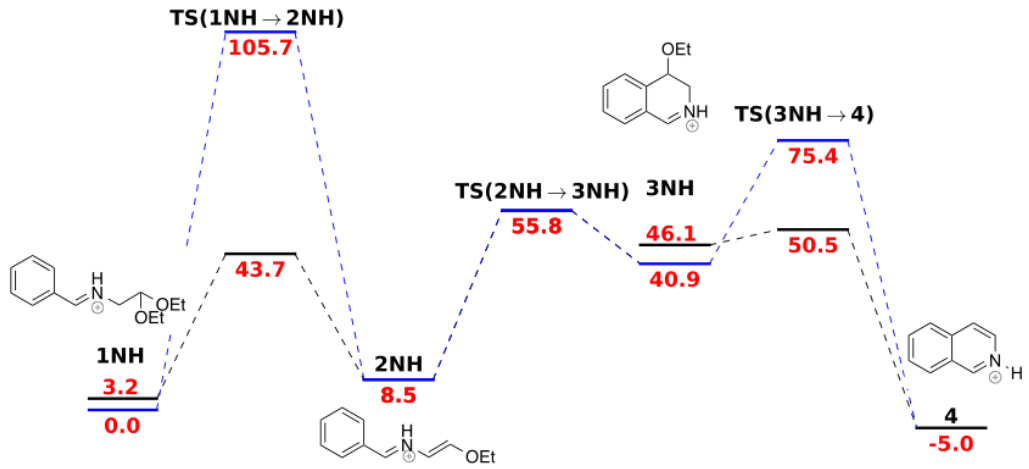

(p) **1NH→2NH→3NH→7NH→4**

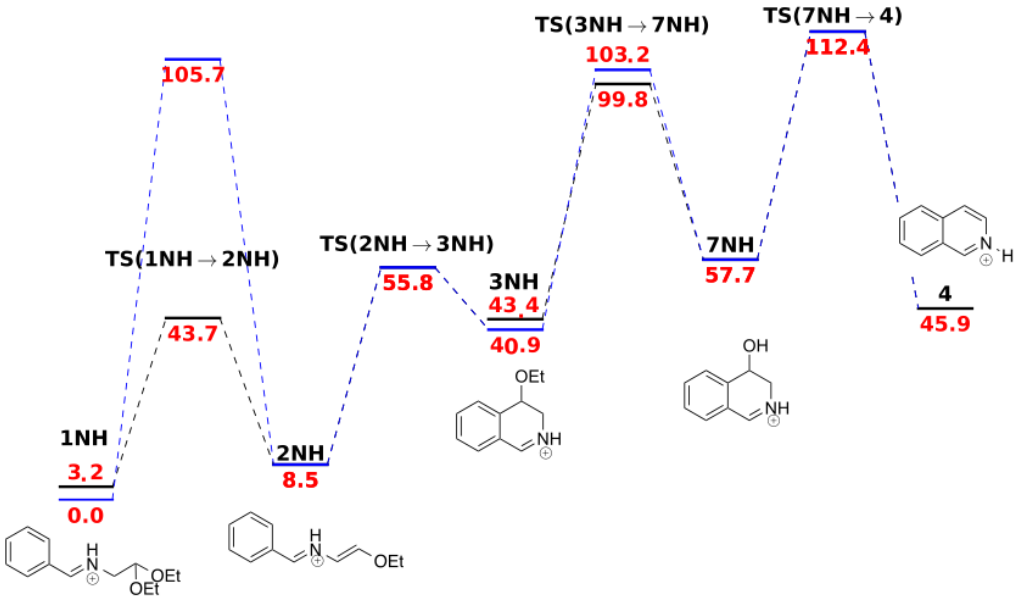

(q) **1NH→2NH→6NH→7NH→4**

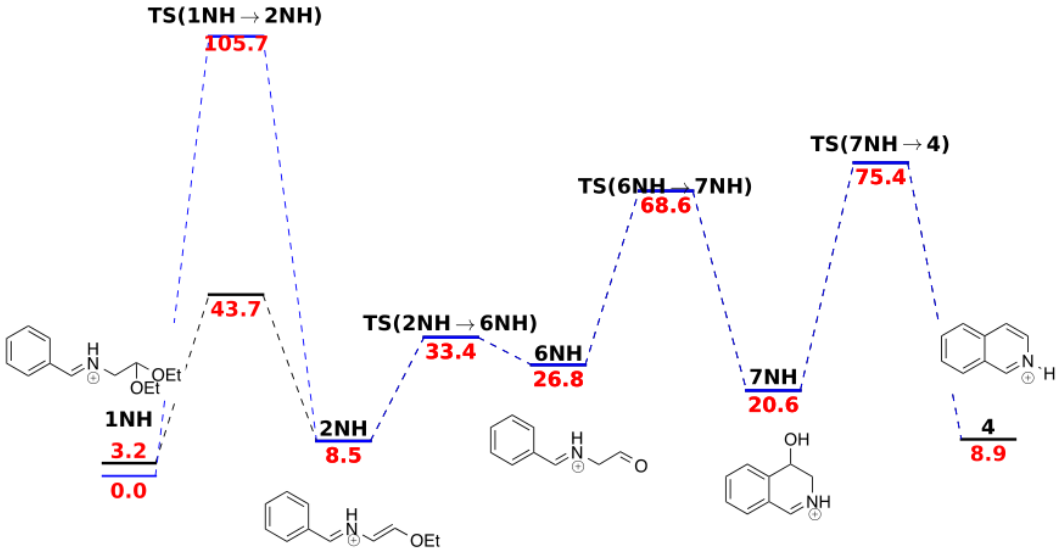

(r) **1NH→5NH→2→3'→3→4**

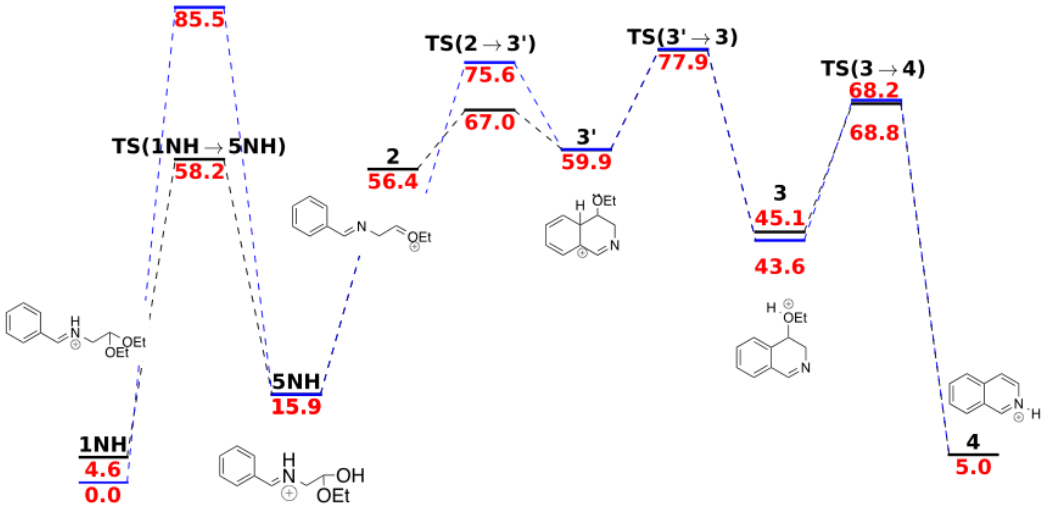

(s) **1NH→5NH→2→3'→3→7→4**

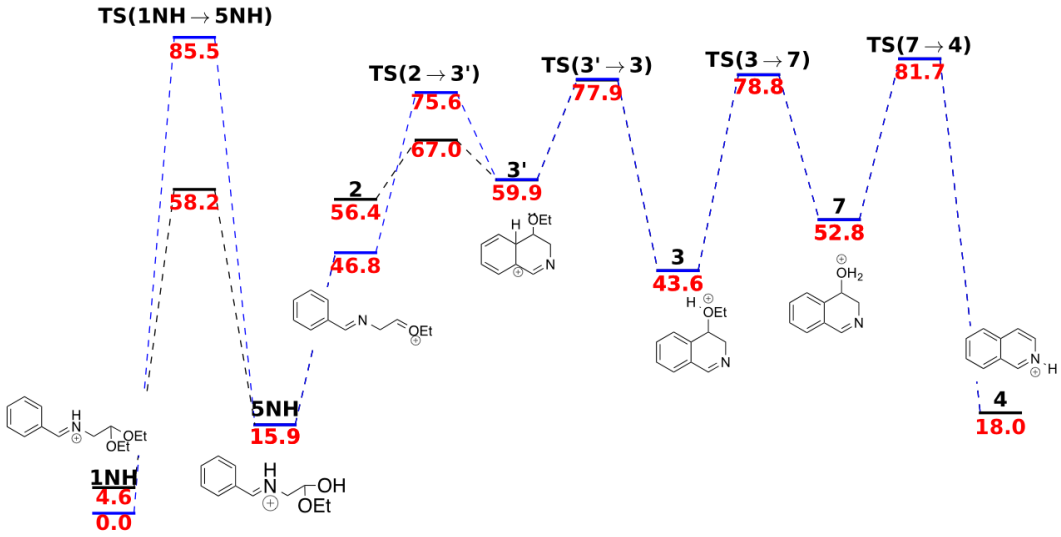

(t) **1NH→5NH→2→6→7→4**

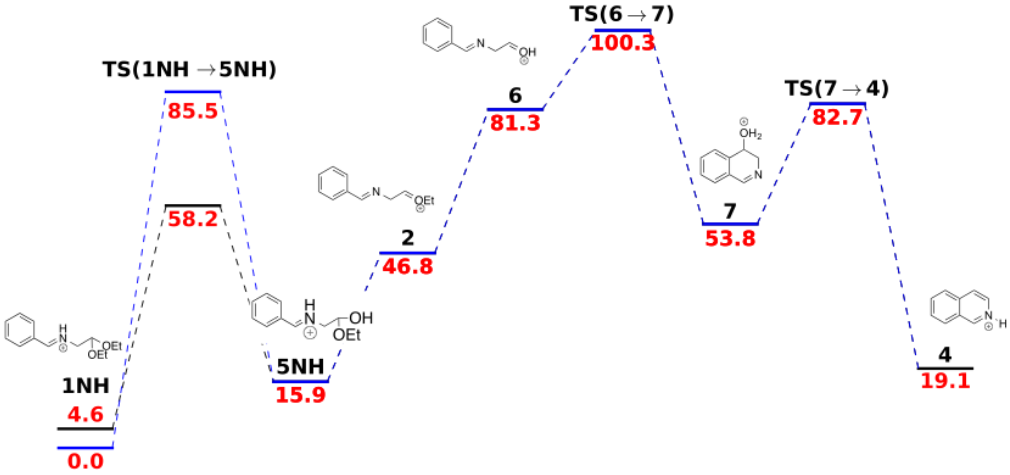

(u) **1NH→5NH→2NH→3NH→4**

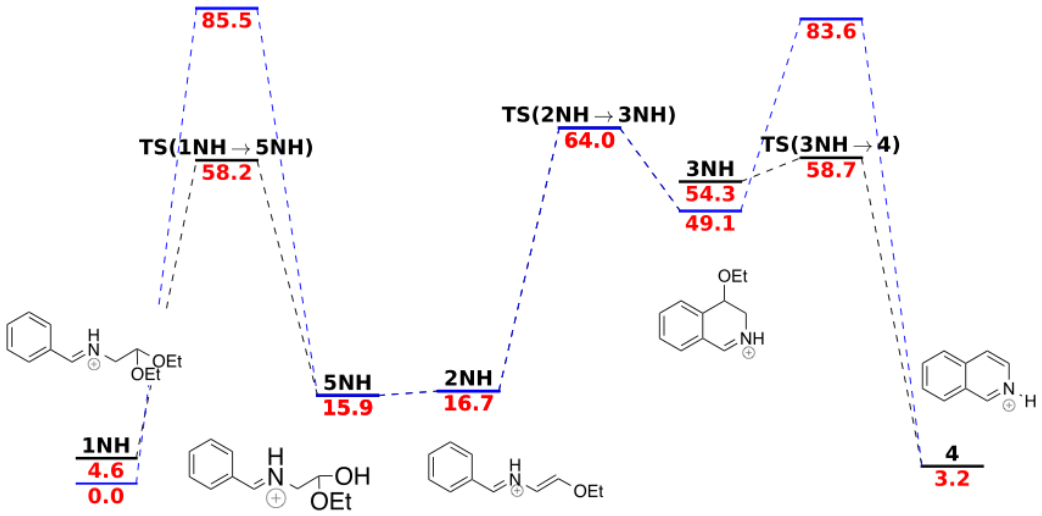

(v) **1NH→5NH→2NH→3NH→7NH→4**

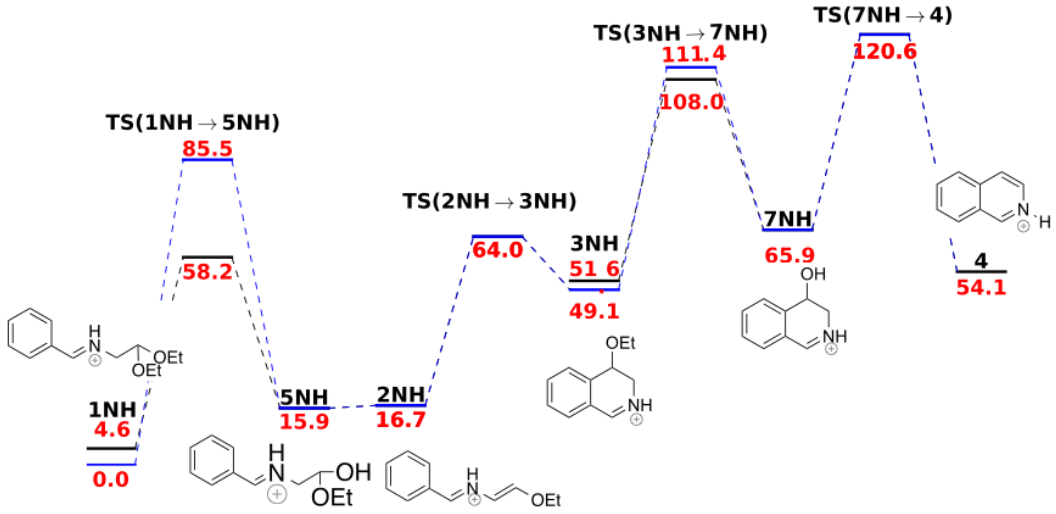

(w) **1NH→5NH→2NH→6NH→7NH→4**

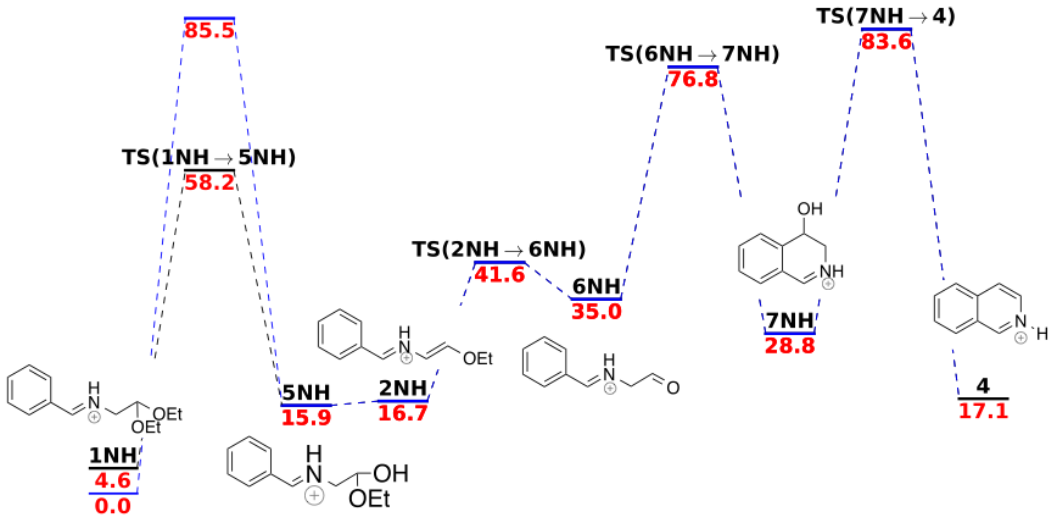

(x) **1NH→5NH→6NH→7NH→4**

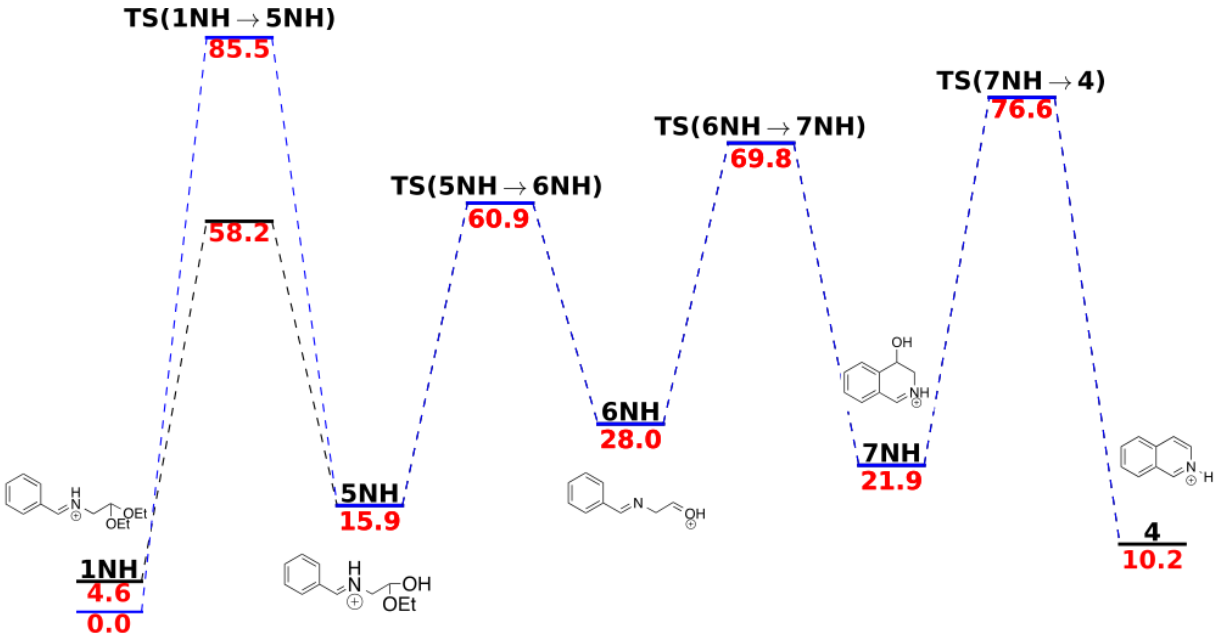

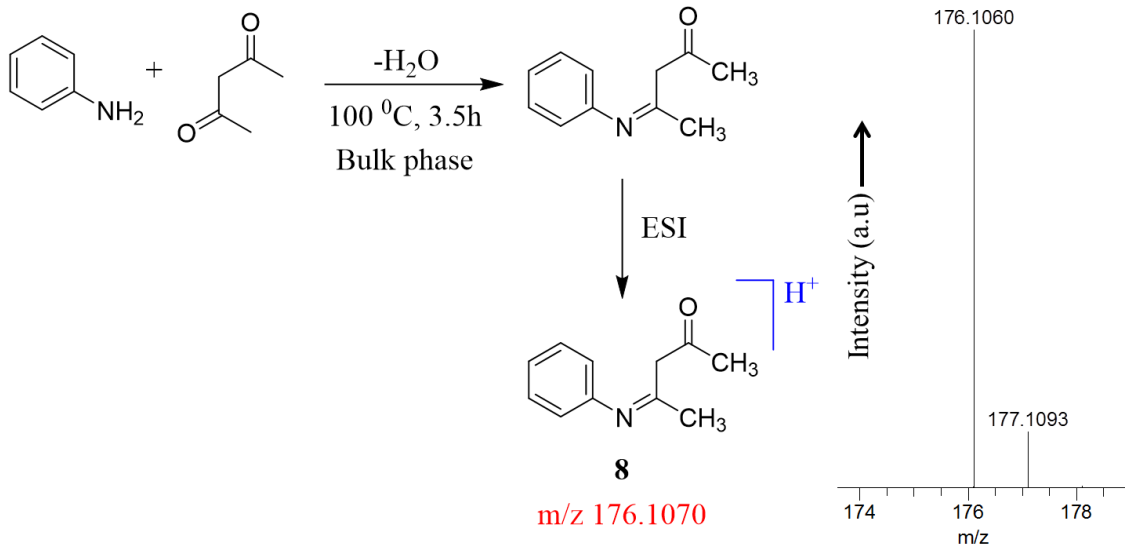

Figure S10. Synthesis of 4-(phenylimino)-2-pentanone in bulk phase followed by electrospray ionization (ESI) to generate the gaseous protonated species **8**, which was detected (right panel ESI-MS) by a high-resolution mass spectrometer. The theoretical *m/z* 176.1070 (in red) for **8** agrees well with the experimentally observed *m/z* 176.1060 for the same species (right panel).

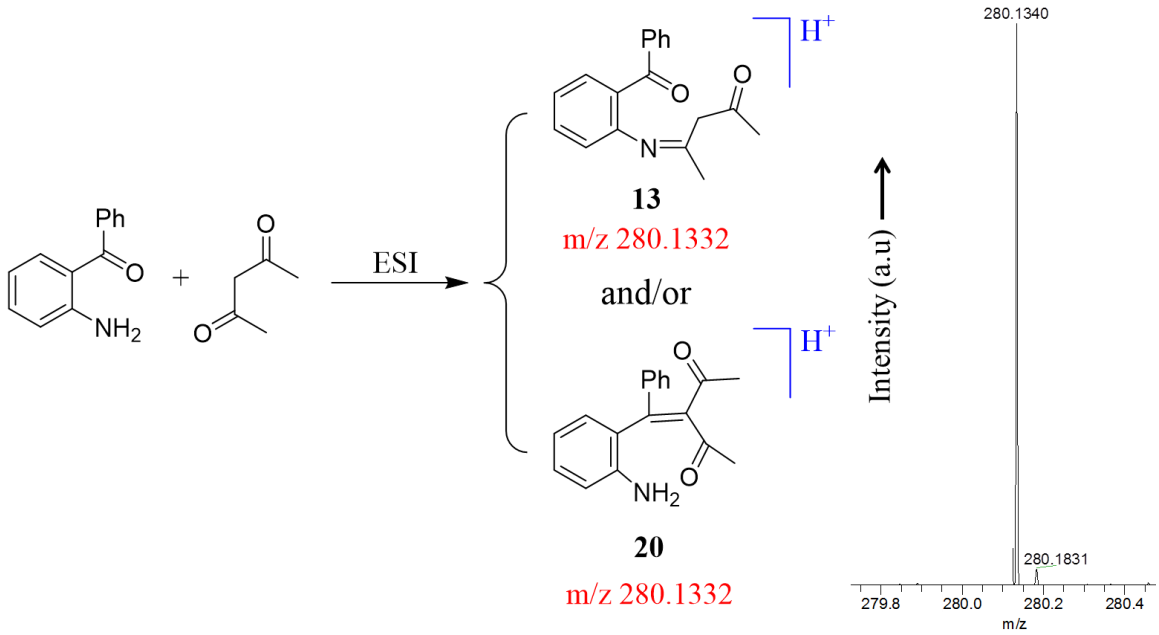

Figure S11. Electrospray-assisted synthesis of the Schiff base **13** and/or the aldol adduct **20** in charged microdroplets followed by their detection in ESI-MS (right panel). The theoretical *m/z* 280.1332 (in red) for **13** or **20** agrees well with the experimentally observed *m/z* 280.1340 for those species (right panel). Being isomeric in nature, **13** and **20** cannot be distinguished by their *m/z* values. However, both of them have been assumed to exist in the gas phase as they were proposed to be the potential intermediates in the Friedländer synthesis of quinoline by the acid-catalyzed reaction of 2-aminobenzophenone and acetylacetone.

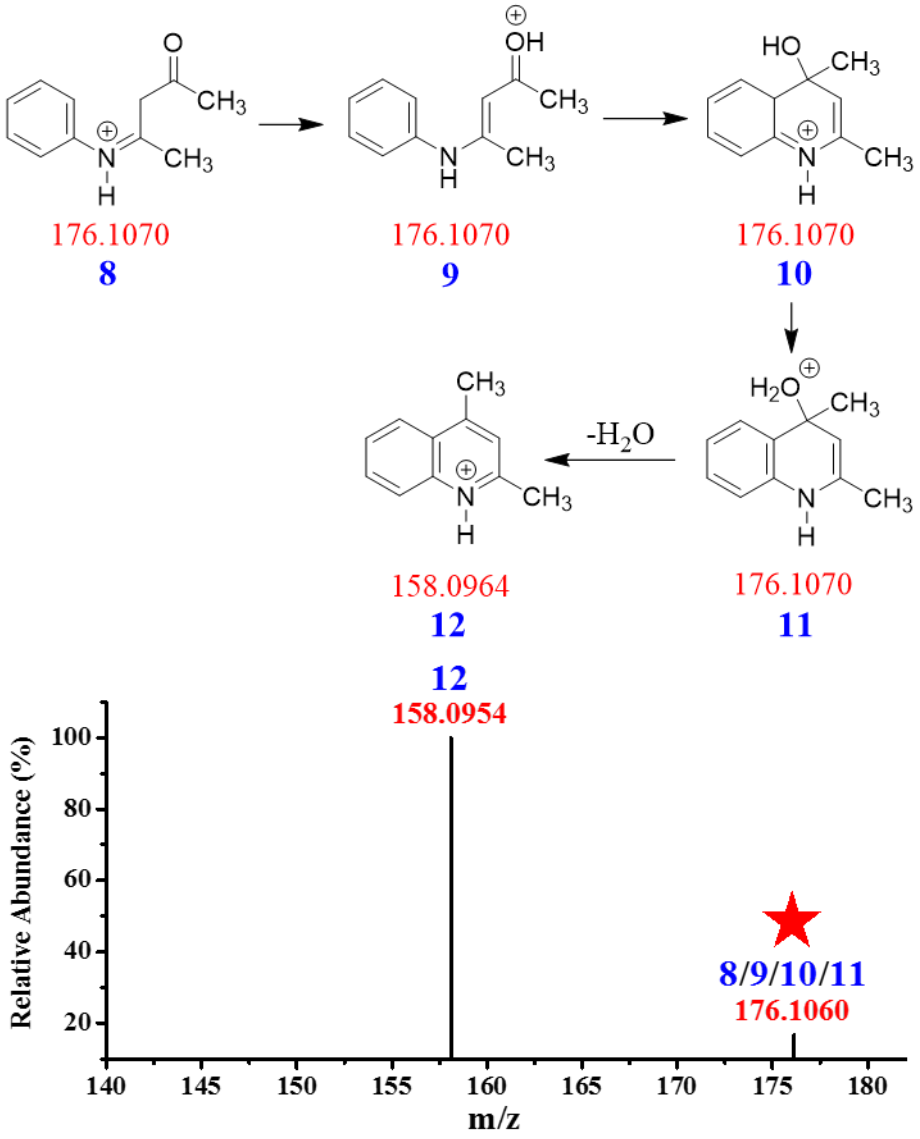

Figure S12. Combes quinoline synthesis in the gas phase upon CID. The upper panel shows the proposed gas-phase synthetic route. The lower panel represents the CID-MS^2 spectrum of the precursor species **8** (*m/z* 176.1060). The activation of **8** is denoted by a star. The theoretical *m/z* values of all species are given in red color below their structures in the scheme (upper panel), which agree well with the experimental *m/z* values shown in the lower panel.

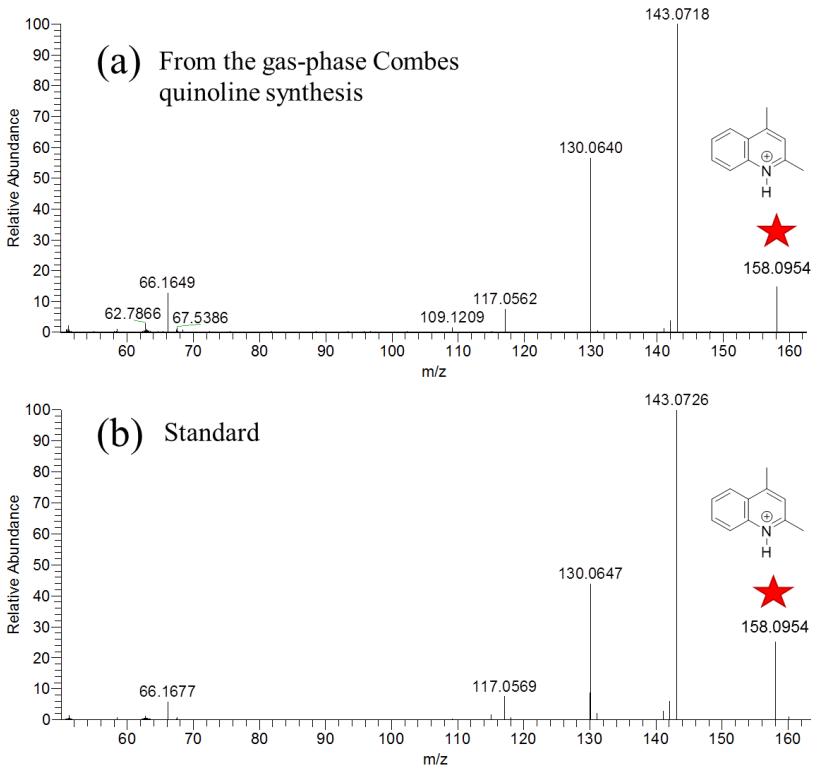

Figure S13. Collision-induced dissociation on the species at *m/z* 158.0954 obtained from (a) the gas-phase Combes quinoline synthesis (Figure S12), and (b) standard 2,4-dimethylquinoline. A star marks the activation of the precursor species by CID.

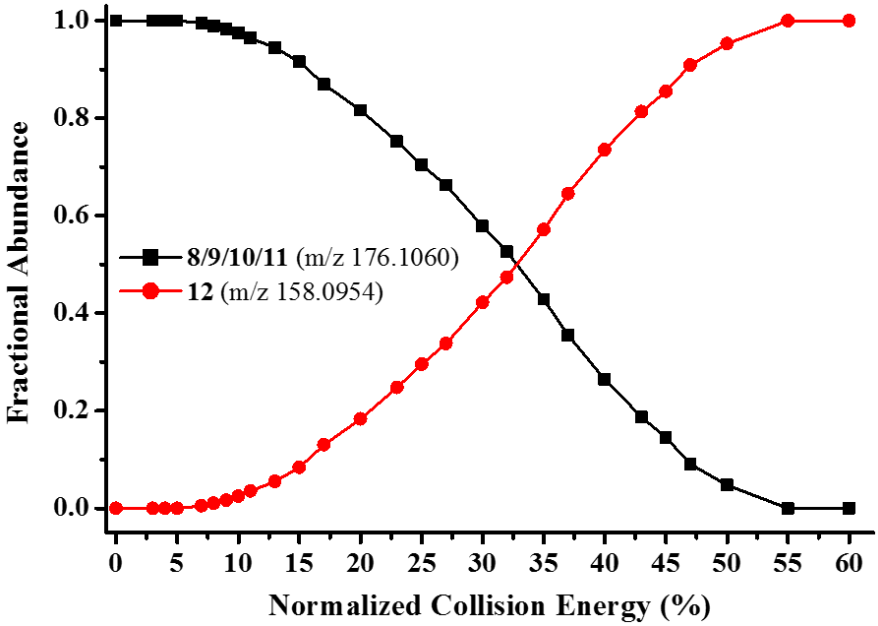

Figure S14. Breakdown curves (energy-resolved transformation profiles) of **8** (*m/z* 176.1060), which produces species **9-12** in MS^2. Species **8-11** are isomeric and cannot be distinguished by their *m/z* values.

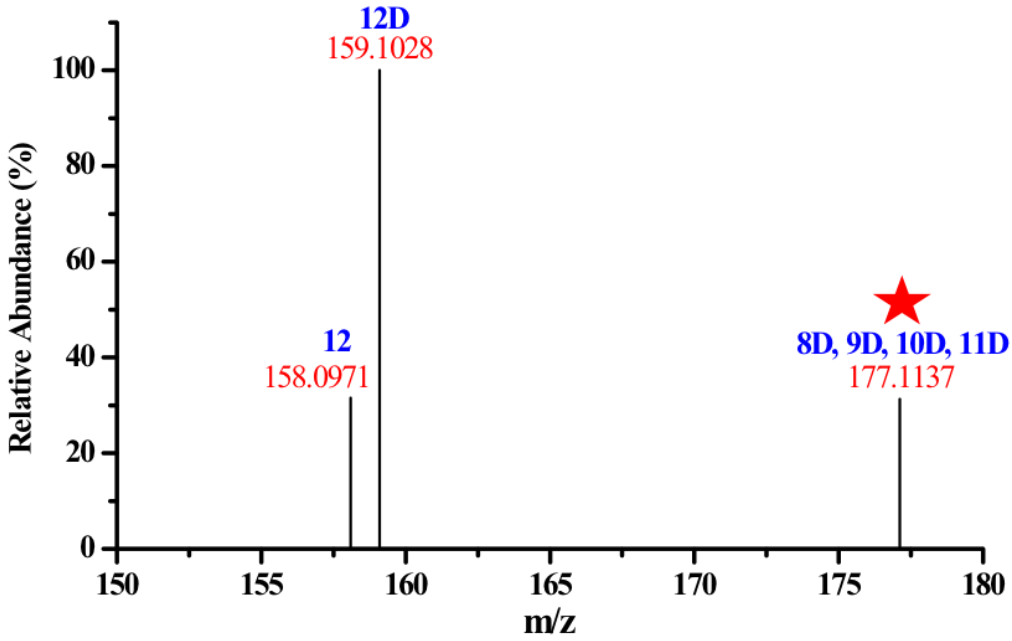

Figure S15. CID-MS^2 of deuterated **8** (**8D**) (*m/z* 177.1137), which produced different deuterated species (**9D**, **10D**, **11D,** and **12D;** see Figure S12; **D** represents that the species is deuterated) as well as the protonated species **12** following the mobile proton model. A star marks the activation of the precursor species by CID. Species **8D**-**11D** are isomeric and cannot be distinguished by their *m/z* values.

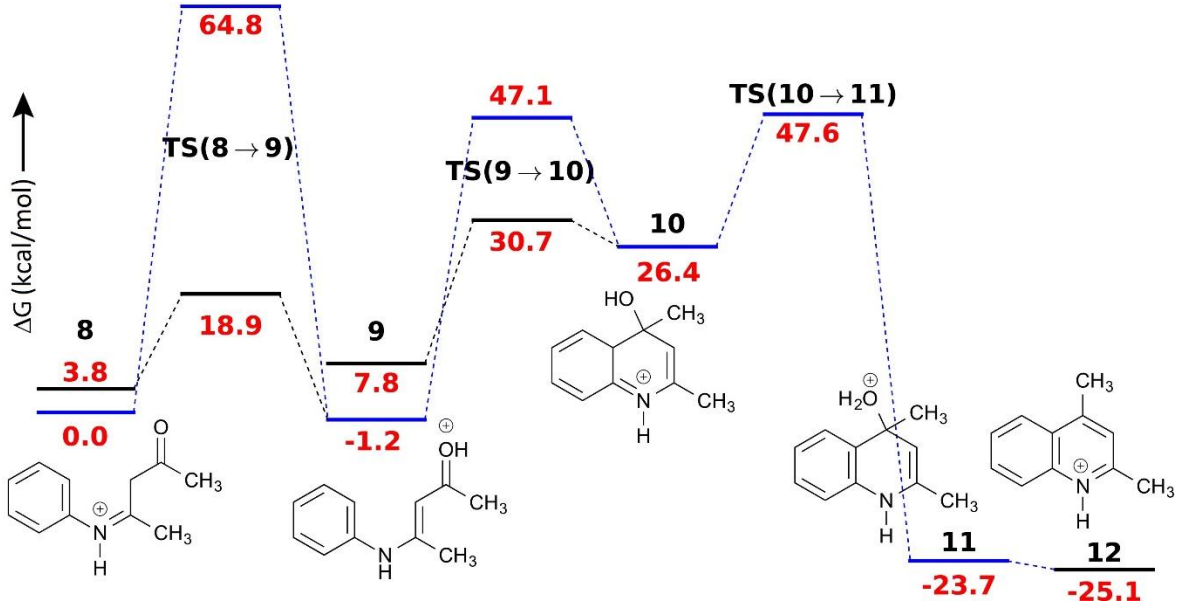

Figure S16. Energy profile of the energetically most preferred route of Combes quinoline synthesis in the gas phase. Black and blue bars stand for conformers participating in path-L and path-S, respectively.

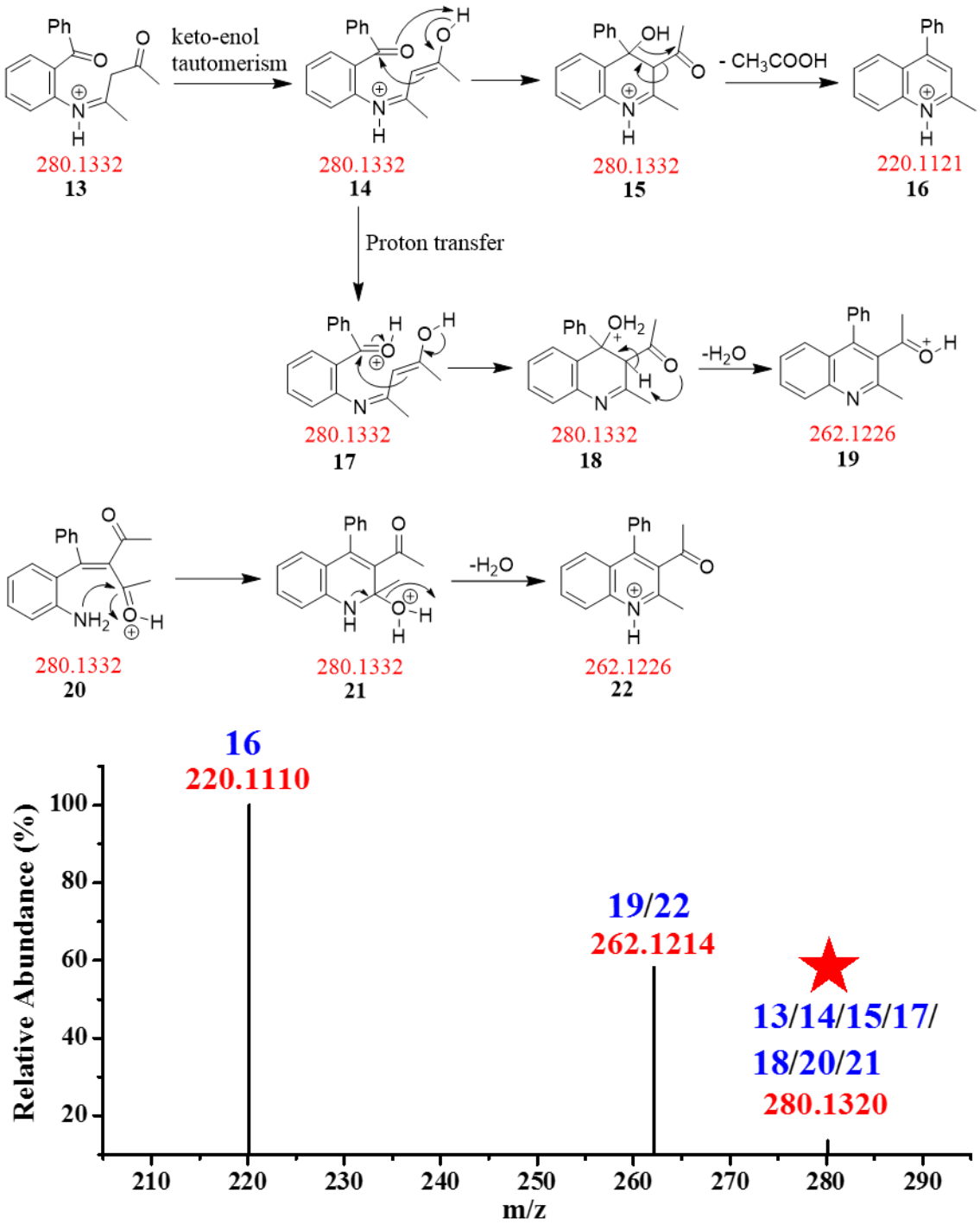

Figure S17. Friedländer quinoline synthesis in the gas phase upon CID. The upper panel shows the proposed gas-phase synthetic route and the lower panel represents the CID-MS^2 spectrum of the precursor species **13** and/or **20** (*m/z* 280.1320). The activations of **13** and/or **20** are denoted by a star. The theoretical *m/z* values of all species are given in red below their structures in the scheme (upper panel), which agree well with the experimental *m/z* values shown in the lower panel.

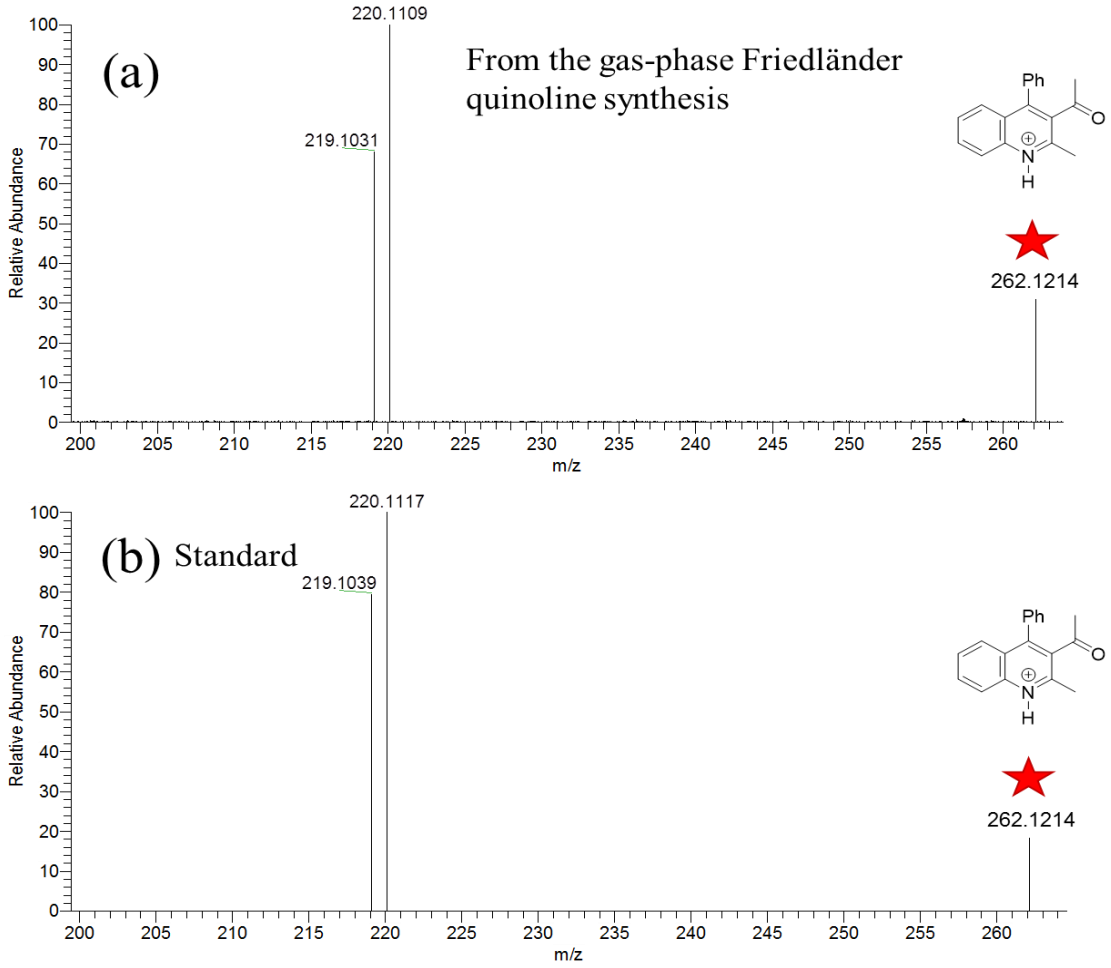

Figure S18. Collision-induced dissociation on the species at *m/z* 262.1214 obtained from (a) the gas-phase Friedländer quinoline synthesis (Figure S17), and (b) standard 2-methyl-3-acetyl-4-phenylquinoline. A star marks the activation of the precursor species by CID.

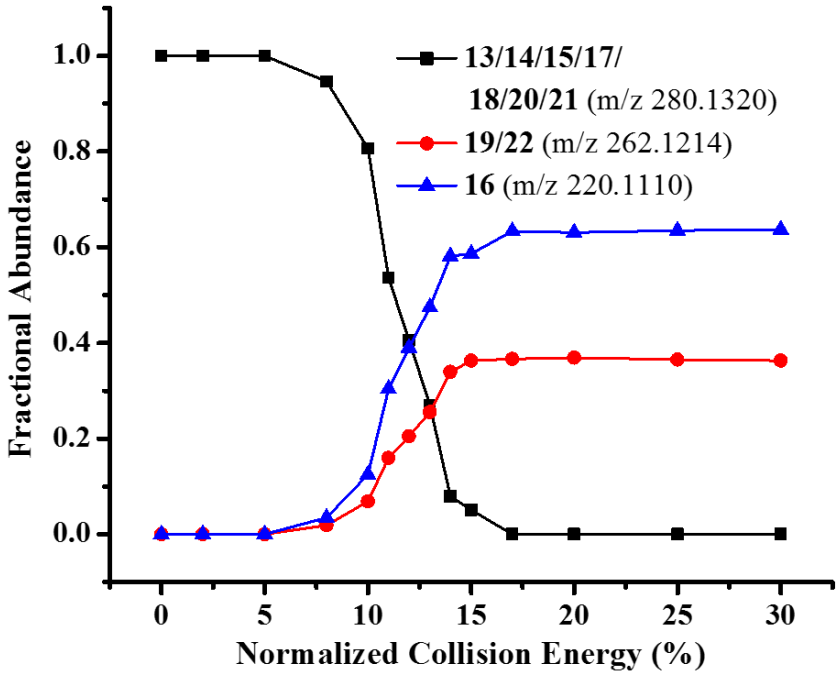

Figure S19. Breakdown curves (energy-resolved transformation profiles) of **13** and/or **20** (*m/z* 280.1320), which produce **14-19**, **21**, and **22** in MS^2. Species **13**, **14**, **15**, **17**, **18**, **20**, and **21** are isomeric and cannot be distinguished by their *m/z* values.

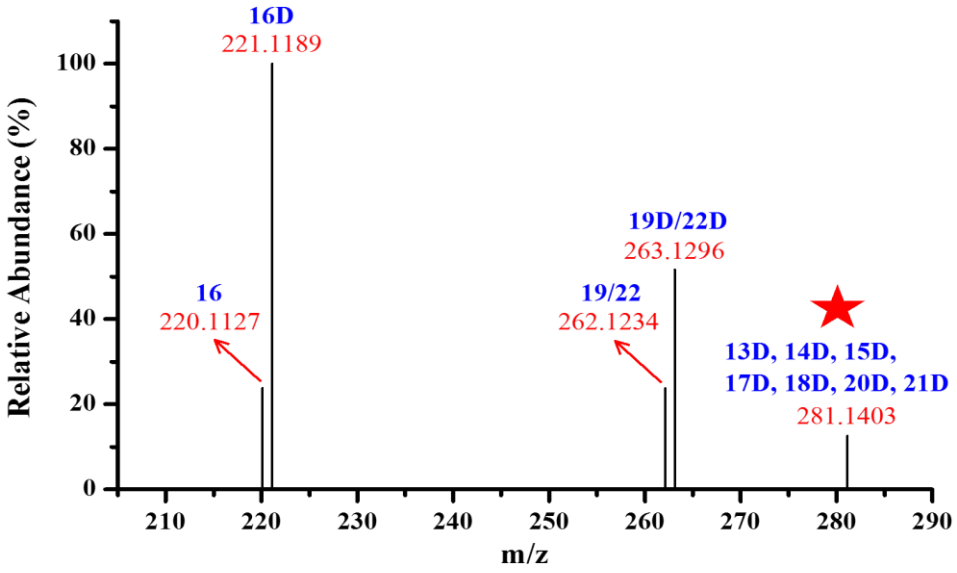

Figure S20. CID-MS^2 of deuterated **13** (**13D**) and/or deuterated **20** (**20D**) (*m/z* 281.1403), which produced different deuterated species (**14D-19D, 21D,** and **22D**; see Figure S17; **D** represents that the species is deuterated) as well as the protonated species **16** and **19/22** following the mobile proton model. A star marks the activation of the precursor species by CID. Species **13D**, **14D**, **15D**, **17D**, **18D**, **20D**, and **21D** are isomeric and cannot be distinguished by their *m/z* values.

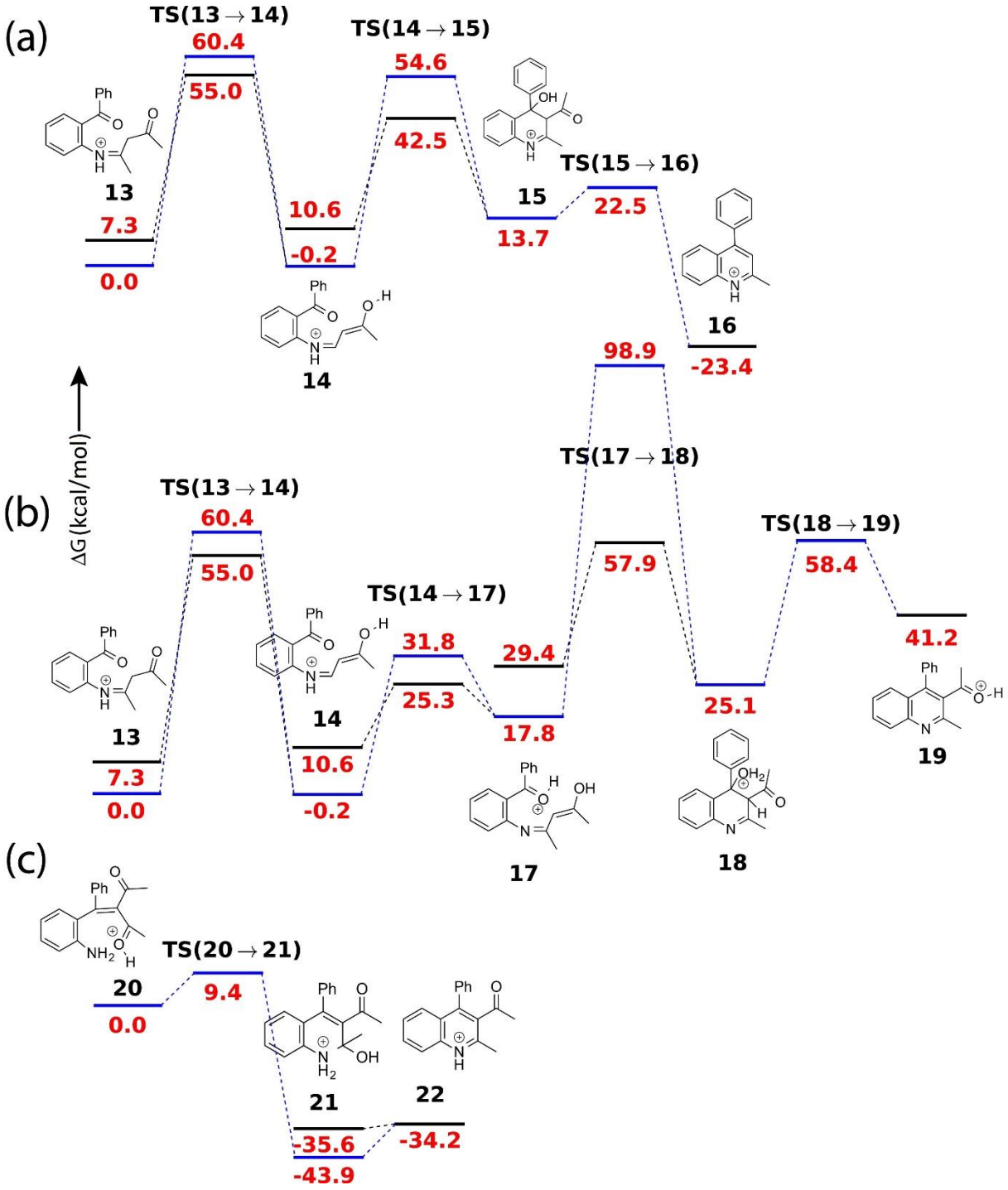

Figure S21. Energy profile of the three routes of Friedländer synthesis of quinolines in the gas phase. Black and blue bars stand for conformers participating in path-L and path-S, respectively.

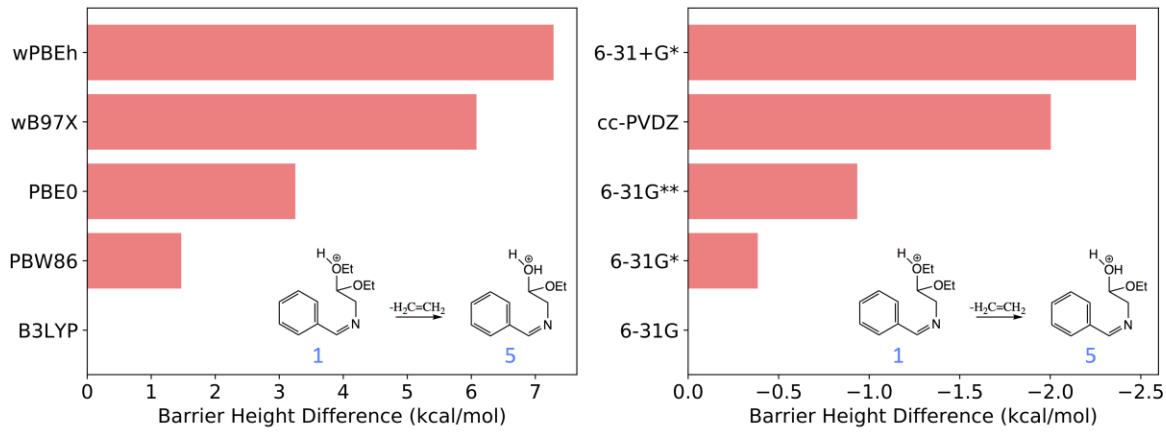

Figure S22. The barrier height for path **1→5** in the Pomeranz-Fritsch synthesis computed with different popular functionals and larger basis sets. B3LYP and 6-31G** were chosen to validate all B3LYP/6-31G calculations.

Table S1. Backtracking results for the gas-phase reaction network of the Pomeranz–Fritsch synthesis of isoquinoline

		Path-L (black path)				**Path-S (blue path)**			
Rea-ctant	Prod-uct	G-reactant (a.u.)	G-transition state (a.u.)	G-product (a.u.)	Barrier (kcal/mol)	G-reactant (a.u.)	G-transition state (a.u.)	G-product (a.u.)	Barrier (kcal/mol)
1NH	**2**	-712.159990	NA	-712.109720	31.5	-712.159990	NA	-712.109720	31.5
5	**6**	-633.537298	-633.488245	-633.498781	30.8	-633.537298	-633.4882451	-633.498781	30.8
3'	**3**	-557.096186	-557.067578	-557.122173	18.0	-557.096080	-557.0673591	-557.124484	18.0
1	**2**	-712.112650	NA	-712.109424	2.0	-712.114439	NA	-712.109281	3.2
1	**5**	-712.112717	-712.0423448	-712.088997	44.2	-712.112717	-712.0423448	-712.088997	44.2
1NH	**2NH**	-712.152239	-712.0877157	-712.143780	40.5	-712.157297	-711.988794	-712.143780	105.7
1NH	**5NH**	-712.150915	-712.0655103	-712.132908	53.6	-712.158249	-712.0219515	-712.135890	85.5
5NH	**2NH**	-633.581871	NA	-633.580624	0.8	-633.581871	NA	-633.580624	0.8
5NH	**2**	-633.582687	NA	-633.533421	30.9	-633.582687	NA	-633.533421	30.9
3NH	**7NH**	-557.108287	-557.0183272	-557.085508	56.5	-557.112283	-557.012932	-557.085909	62.3
7	**4**	-478.557785	-478.5117309	-478.613114	28.9	-478.557785	-478.511731	-478.613114	28.9
7NH	**4**	-478.594457	-478.5072262	-478.613146	54.7	-478.594457	-478.507226	-478.613146	54.7
5	**2**	-633.536229	-633.4922175	-633.524982	27.6	-633.536229	-633.492218	-633.524982	27.6
1	**5NH**	-712.113989	-712.0638232	-712.134694	31.5	-712.113989	-712.063823	-712.134694	31.5
6	**7**	-478.513538	-478.4832616	-478.557367	19.0	-478.513538	-478.483262	-478.557367	19.0
2	**6**	-557.115458	-557.0605237	-557.060524	34.5	-557.115458	-557.060524	-557.076433	34.5
2NH	**6NH**	-557.164069	-557.1243209	-557.134902	24.9	-557.164069	-557.124321	-557.134902	24.9
6NH	**7NH**	-478.584526	-478.5179112	-478.594342	41.8	-478.584526	-478.517911	-478.594342	41.8
2	**3'**	-557.100635	-557.0836991	-557.094982	10.6	-557.115939	-557.070077	-557.122789	28.8
2NH	**3NH**	-557.164153	-557.0887383	-557.112537	47.3	-557.164153	-557.088738	-557.112537	47.3
5NH	**6NH**	-633.582231	-633.5104964	-633.562889	45.0	-633.582231	-633.510496	-633.562889	45.0
3NH	**4**	-557.103884	-557.0970167	-557.185452	4.3	-557.112285	-557.057261	-557.185420	34.5
3	**7**	-557.122438	-557.0663215	-557.107826	35.2	-557.122438	-557.066322	-557.107826	35.2
3	**4**	-557.121700	-557.0849227	-557.185565	23.1	-557.124136	-557.083930	-557.186205	25.2

Table S2. Rate-determining step (r.d.s.) in each route of the gas-phase reaction network of the Pomeranz–Fritsch synthesis of isoquinoline

Paths	r.d.s.	r.d.s. barrier (kcal/mol)
1 -- 2 -- 3' -- 3 -- 4	3--4	23.08
1 -- 5NH -- 2 -- 3' -- 3 -- 4	1--5NH	31.48
1NH -- 2 -- 3' -- 3 -- 4	1NH--2	31.54
1NH -- 2 -- 6 -- 7 -- 4	2--6	34.47
1 -- 2 -- 6 -- 7 -- 4	2--6	34.47
1 -- 5NH -- 2 -- 6 -- 7 -- 4	2--6	34.47
1NH -- 2 -- 3' -- 3 -- 7 -- 4	3--7	35.21
1 -- 2 -- 3' -- 3 -- 7 -- 4	3--7	35.21
1 -- 5NH -- 2 -- 3' -- 3 -- 7 -- 4	3--7	35.21
1 -- 5 -- 2 -- 6 -- 7 -- 4	1--5	44.16
1 -- 5 -- 2 -- 3' -- 3 -- 4	1--5	44.16
1 -- 5 -- 2 -- 3' -- 3 -- 7 -- 4	1--5	44.16
1 -- 5 -- 6 -- 7 -- 4	1--5	44.16
1NH -- 2NH -- 3NH -- 4	2NH--3NH	47.32
1 -- 5NH -- 2NH -- 3NH -- 4	2NH--3NH	47.32
1NH -- 5NH -- 2NH -- 3NH -- 4	1NH--5NH	53.59
1NH -- 5NH -- 2 -- 6 -- 7 -- 4	1NH--5NH	53.59
1NH -- 5NH -- 2 -- 3' -- 3 -- 4	1NH--5NH	53.59
1NH -- 5NH -- 2 -- 3' -- 3 -- 7 -- 4	1NH--5NH	53.59
1NH -- 2NH -- 6NH -- 7NH -- 4	7NH--4	54.74
1NH -- 5NH -- 2NH -- 6NH -- 7NH -- 4	7NH--4	54.74
1NH -- 5NH -- 6NH -- 7NH -- 4	7NH--4	54.74
1 -- 5NH -- 2NH -- 6NH -- 7NH -- 4	7NH--4	54.74
1 -- 5NH -- 6NH -- 7NH -- 4	7NH--4	54.74
1NH -- 2NH -- 3NH -- 7NH -- 4	3NH--7NH	56.45
1NH -- 5NH -- 2NH -- 3NH -- 7NH -- 4	3NH--7NH	56.45
1 -- 5NH -- 2NH -- 3NH -- 7NH -- 4	3NH--7NH	56.45

Table S3. Backtracking results for the Combes quinoline synthesis in the gas phase

		Path-L (black path)				Path-S (blue path)			
Reactant	Product	G-reactant (a.u.)	G-transition state (a.u.)	G-product (a.u.)	Barrier (kcal/mol)	G-reactant (a.u.)	G-transition state (a.u.)	G-product (a.u.)	Barrier (kcal/mol)
11	**12**	-557.059739	NA	-557.061956	-1.4	-557.059739	NA	-557.061956	-1.4
10	**11**	-556.979844	-556.946100	-557.059773	21.2	-556.979844	-556.946100	-557.059773	21.2
9	**10**	-557.009625	-556.973115	-556.979925	22.9	-557.023923	-556.947057	-556.979780	48.2
8	**9**	-557.016040	-556.991897	-557.023897	15.2	-557.022032	-556.918730	-557.023955	64.8

Table S4. Backtracking results for the Friedländer synthesis of quinoline in the gas phase.

		Path-L (black path)				Path-S (blue path)			
Reactant	Product	G-reactant (a.u.)	G-transition state (a.u.)	G-product (a.u.)	Barrier (kcal/mol)	G-reactant (a.u.)	G-transition state (a.u.)	G-product (a.u.)	Barrier (kcal/mol)
15	**16**	-901.217574	-901.203447	-901.276591	8.9	-901.217574	-901.203447	-901.276591	8.9
14	**15**	-901.224840	-901.174048	-901.220005	31.9	-901.242161	-901.154863	-901.219799	54.8
13	**14**	-901.230089	-901.154066	-901.242085	47.7	-901.241732	-901.145523	-901.242147	60.4
18	**19**	-901.201559	-901.148509	-901.175946	33.3	-901.201559	-901.148509	-901.175946	33.3
17	**18**	-901.194788	-901.149309	-901.201568	28.5	-901.213337	-901.084077	-901.201542	81.1
14	**17**	-901.224840	-901.201535	-901.213513	14.6	-901.242161	-901.191183	-901.213400	32.0
21	**22**	-901.262694	NA	-901.260477	1.4	-901.275920	NA	-901.260325	9.8
20	**21**	-901.206298	-901.191332	-901.276241	9.4	-901.206298	-901.191332	-901.276241	9.4

References

(1) Gensler, W. J. In *Organic Reactions*; John Wiley & Sons, Inc.: New York, **2004**.
(2) Banerjee, S.; Zare, R. N. *Angew. Chem. Int. Ed.* **2015**, *54*, 14795.
(3) Marco-Contelles, J.; Pérez-Mayoral, E.; Samadi, A.; Carreiras, M. d. C.; Soriano, E. *Chem. Rev.* **2009**, *109*, 2652.
(4) Cole, R. B. *Electrospray and MALDI Mass Spectrometry*; John Wiley & Sons: New Jersey, **2010**.
(5) See http://tools.thermofisher.com/content/sfs/brochures/PSB104-Normalized-Collision-Energy-Technology-EN.pdf, Accessed 6-29-17.
(6) O'Boyle, N. M.; Banck, M.; James, C. A.; Morley, C.; Vandermeersch, T.; Hutchison, G. R. *J. Cheminf.* **2011**, *3*, 33.
(7) O'Boyle, N. M.; Morley, C.; Hutchison, G. R. *Chem. Cent. J.* **2008**, *2*, 5.
(8) Ufimtsev, I.S. and Martínez, T.; *J. Chem. Theo.Comp.* **2009**, 5, 2619.
(9) Shao, Y. et al.; *Mol. Phys.* **2015**, 113, 184-215.
(10) Weinan, E.; Ren, W. Q.; Vanden-Eijnden, E. *Phys. Rev. B* **2002**, *66*.
(11) Kordel, E.; Villani, C.; Klopper, W. *Mol. Phys.* **2007**, *105*, 2565.
(12) Henkelman, G.; *J. Chem. Phys.* **2000**, 113, 9901.
(13) Sleno, L.; Volmer, D. A. *J. Mass Spectrom.* **2004**, *39*, 1091.
(14) McLuckey, S. A. *J. Am. Soc. Mass Spectrom.* **1992**, *3*, 599.
(15) Fisher, E. R.; Kickel, B. L.; Armentrout, P. B. *J. Phy. Chem.* **1993**, *97*, 10204.
(16) Mitchell Wells, J.; McLuckey, S. A. In *Methods in Enzymology*; Academic Press: Cambridge, **2005**; Vol. Volume 402, p 148.
(17) Cheng, C.; Gross, M. L. *Mass Spectrom. Rev.* **2000**, *19*, 398.
(18) Wang, H.-Y.; Zhang, X.; Guo, Y.-L.; Tang, Q.-H.; Lu, L. *J. Am. Soc. Mass Spectrom.* **2006**, *17*, 253.
(19) Pruesse, T.; Fiedler, A.; Schwarz, H. *J. Am. Chem. Soc.* **1991**, *113*, 8335.
(20) Glish, G. L.; Cooks, R. G. *J. Am. Chem. Soc.* **1978**, *100*, 6720.
(21) Li, J. J. *Name Reactions: A Collection of Detailed Mechanisms and Synthetic Applications Fifth Edition*; Springer International Publishing: Switzerland, **2014**.
(22) Born, J. L. *J. Org. Chem.* **1972**, *37*, 3952.
(23) Yamashkin, S. A.; Yudin, L. G.; Kost, A. N. *Chem Heterocycl Compd* **1992**, *28*, 845.
(24) Dongré, A. R.; Jones, J. L.; Somogyi, Á.; Wysocki, V. H. *J. Am. Chem. Soc.* **1996**, *118*, 8365.
(25) Banerjee, S.; Mazumdar, S. *Int. J. Anal. Chem.* **2012**, *2012*, *1*.
(26) Cheng, C.-C.; Yan, S.-J. In *Organic Reactions*; John Wiley & Sons, Inc.: New York, **2004**.